Article

Highly Potent and Selective Butyrylcholinesterase Inhibitors for Cognitive Improvement and Neuroprotection

Qi Li, Ying Chen, Shuaishuai Xing, Qinghong Liao, Baichen Xiong, Yuanyuan Wang, Weixuan Lu, Siyu He, Feng Feng, Wenyuan Liu,* Yao Chen,* and Haopeng Sun*

Read Online

ACCESS | Metrics & More | Article Recommendations | Supporting Information

ABSTRACT: Butyrylcholinesterase (BChE) has been considered as a potential therapeutic target for Alzheimer's disease (AD) because of its compensation capacity to hydrolyze acetylcholine (ACh) and its close association with $A\beta$ deposit. Here, we identified **S06-1011** (hBChE IC$_{50}$ = 16 nM) and **S06-1031** (hBChE IC$_{50}$ = 25 nM) as highly effective and selective BChE inhibitors, which were proved to be safe and long-acting. Candidate compounds exhibited neuroprotective effects and the ability to improve cognition in scopolamine- and $A\beta_{1-42}$ peptide-induced cognitive deficit models. The best candidate **S06-1011** increased the level of ghrelin, a substrate of BChE, which can function as improving the mental mood appetite. The weight gain of the **S06-1011**-treated group remarkably increased. Hence, BChE inhibition not only plays a protective role against dementia but also exerts a great effect on treating and nursing care.
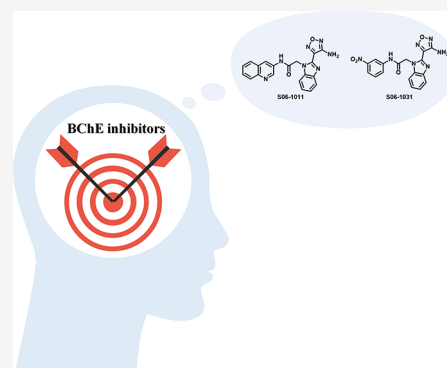
1. INTRODUCTION

Alzheimer's disease (AD) is a progressive neurodegenerative disorder, characterized by central cognitive and behavioral dysfunction.[1] As reported by the World Alzheimer Report 2018, 50 million people are affected by dementia, and this number will more than triple to 152 million by 2050.[2] Although the exact etiology of AD has not been completely understood, several common hallmarks, including cholinergic dysfunction, amyloid-β ($A\beta$) deposits, τ-protein aggregation, neuroinflammation, and mitochondrial dysfunction, are considered to be closely related to the pathophysiology and progression of AD.[3−7] Due to the complexity of AD pathology, large investments result in low returns, and few drugs have been clinically applied for AD treatment.[1,2] Except for memantine, an N-methyl-D-aspartic acid receptor (NMDAR) blocker, all other approved drugs benefit the dysfunctional neurocholinergic system.[8−11] From this point of view, designing cholinesterases (ChE) inhibitors remains a reasonable and promising strategy for AD treatment.

According to the cholinergic hypothesis, damaged nerve cells in the AD brain, especially in the cortex and hippocampus, forebrain Meynert basal ganglia, and septal area, lead to an abnormal decrease in acetylcholine (ACh).[12−14] Low levels of ACh are a symbolic pathological feature of AD, particularly for its strong association with cognitive function.[15] There are two ChEs named acetylcholinesterase (AChE EC 3.1.1.7) and butyrylcholinesterase (BChE, EC 3.1.1.8), but ACh is predominantly decomposed by the former under physiological conditions.[16] Normally, AChE is predominant in muscles and the nervous system accompanied by a lower level of BChE.[17] BChE is notably synthesized in the liver and secreted into the plasma. Neural BChE is mostly of glial origin.[18] However, the compensatory character of BChE is greatly noticeable under pathological conditions. In the AChE-knockout mouse model, BChE was proven to compensate for hydrolyzing ACh due to the lack of AChE, thereby maintaining normal cholinergic pathways.[18,19] In progressed AD, the level of AChE in the brain sharply declines by 90%, while BChE increases to 165% of normal levels, taking over the hydrolysis of ACh.[20] Hence, BChE is a potential target for the treatment of advanced AD. Generally, central nervous system (CNS) drugs are required for good blood−brain barrier (BBB) penetration capacity; however, most drugs suffer from the restriction of tissue selectivity, which commonly leads to peripheral side effects. Existing selective AChE and nonselective ChE inhibitors exhibit typical cholinergic toxicity, such as nausea and vomiting, due to inhibition of peripheral AChE by residues.[21] Furthermore, there are no physiological deficiencies in BChE-knockout mice, and people with silent BChE can live healthily to an old age.[22,23] Based on these facts, suppression of BChE shows an advantage in drug safety for AD treatment.

In addition to cholinergic benefits, BChE has been demonstrated to be highly related to $A\beta$.[24] Histochemical localization has proven that BChE deposition is strongly
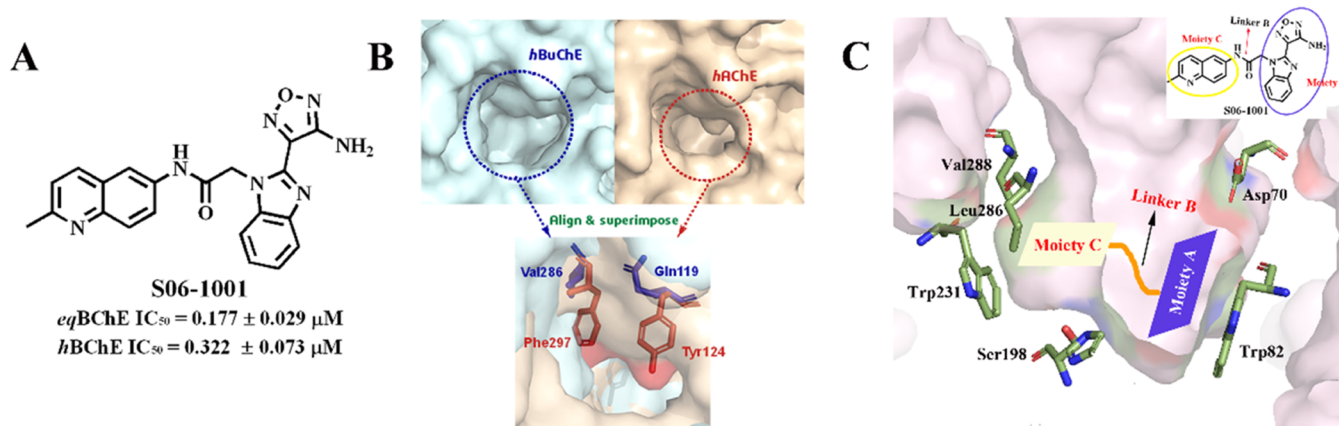
Figure 1. (A) Chemical structure of the lead compound **S06-1001**. (B) Substrate-binding pockets and superimposition of *h*AChE (PDB code: 4ey4) and *h*BChE (PDB code: 1p0i). Residues (Phe297 and Tyr124) of *h*AChE are represented in red, and residues (Val288 and Gln119) of *h*BChE are in blue. (C) Molecular dynamic result of **S06-1001** and modification strategy purposed for further derivative design.

associated with progressive Aβ aggregation in senile plaques.[25] Moreover, Aβ fibers in the brain were remarkably reduced in the BChE-knockout mouse model, indicating that BChE may promote Aβ deposition.[26] The cognition of BChE-knockout mice was found to not be influenced by injection of neurotoxic Aβ_{25-35}, whereas wild-type mice suffered from cognitive insults after administration.[27] From this point of view, BChE inhibition can be an effective strategy for Aβ clearance.

AD is an age-related neurodisease; AD patients often have metabolic dysfunction. Epidemiological studies have validated that some diseases, such as metabolic syndrome, are also risk factors for elderly AD patients.[28,29] Weight loss has been identified as a common syndrome in AD patients and appears even earlier than damages in cognitive functions.[30] It has been demonstrated that weight gain may afford protection against dementia, but this can be tough for AD patients owing to the poor mental state.[31] In 2004, Brimijoin et al. reported the function of BChE as hydrolyzing ghrelin through the removal of the octanoyl group.[32] Ghrelin, a 28-amino acid peptide, plays an essential role in energy homeostasis and metabolism.[33,34] It is secreted from the fundus of the human stomach and the pancreas. Ghrelin is capable of penetrating the BBB and plays a significant role in neurotrophy, particularly in the hippocampus.[35] It is essential for improving cognitive adaptation to the environment and the learning process and elevating mental mood and appetite.[36−38] Based on the hydrolysis influence of BChE on ghrelin, BChE inhibition may help improve appetite and food intake, which is a great benefit for AD patients. Moreover, elevated appetite of patients is helpful in ameliorating their nutrition state, which greatly reduces the pressure on caregivers.

As concluded, selective BChE inhibitors are of vital importance to prolonging the onset time, removing abnormal brain Aβ deposits, protecting neural cells against oxidative stress, evading adverse effects, and improving the mood and nutrition state of patients, which are all beneficial for AD treatment. Previously, a novel compound **8012-9656** (**S06-1001**, Figure 1A) was reported by our group to exhibit nanomolar-range inhibitory activity (*ee*AChE IC$_{50}$ > 100 μM, *eq*BChE IC$_{50}$ = 0.18 ± 0.03 μM, *h*BChE IC$_{50}$ = 0.32 ± 0.07 μM) and high selectivity (AChE IC$_{50}$/BChE IC$_{50}$ ratio > 500).[39] Herein, taking **S06-1001** as the lead, we report the medicinal chemistry optimization of this compound, including both activity and druglike properties. During this process, two compounds, **S06-**

1011 and **S06-1031** containing a 3-(benzoimidazol-2-yl)-1,2,5-oxadiazole core, were identified as drug candidates for a new structural class of highly selective BChE inhibitors.

2. RESULTS AND DISCUSSION

2.1. Design, Synthesis, and Enzymic Inhibition Screening of Selective BChE Inhibitors. To better design the derivatives, we first thoroughly explored the structure of BChE and its structural differences from that of AChE. Generally, the overall structures for the two ChEs are similar.[21] Both enzymes, which share more than 50% homology, contain a catalytic active site (CAS), a deep and narrow gorge, and a peripheral anionic site (PAS).[40] Despite the high structural similarity, the subtle but pivotal residue differences in substrate-binding pockets provide an opportunity to exploit selective inhibitors. As shown in Figure 1B, larger residues of *h*AChE, such as Phe297 and Tyr124, protrude into the pocket, resulting in the formation of a narrower site, while smaller residues of *h*BChE, such as Gln119 and Val286, create a wider cavity for ligands to bind to. This structural difference dictates the substrate specificity of two enzymes: AChE tends to bind small molecules such as ACh; as a counterpart, BChE can hydrolyze various neuroactive peptides due to its broader space for substrates.[41]

Based on the cocrystal structure of *h*BChE, we previously discovered a lead compound **S06-1001** with moderate BChE inhibitory ability and high selectivity.[39] According to the molecular dynamics (MD) simulation result of **S06-1001** (Supporting Information, Figure S1), an intramolecular hydrogen bond was formed between the N atom of benzimidazole and the primary amino group on the oxadiazole, further constituting a large polyaromatic-ring structure. This structure was involved in a parallel π−π stacking interaction with Trp82 (Figure 1C), which was a dominating residue for intermolecular interaction between the compound and BChE. The subpocket at the bottom of the gorge is pivotal to distinguish the two ChEs, and it is also predominant in the design of highly selective inhibitors. Based on the MD results obtained for **S06-1001**, we hypothesized that the quinoline ring could be inserted into this pocket (Figure 1C), contributing to the high selectivity of **S06-1001**. Therefore, we proposed a modification strategy (Moiety A, Linker B, and Moiety C) to support our speculation and attempted to design and develop derivatives with higher activity and selectivity.

Scheme 1. General Procedure for the Preparation of Terminal Compounds S06-1002, S06-1007, and S06-1008[a]
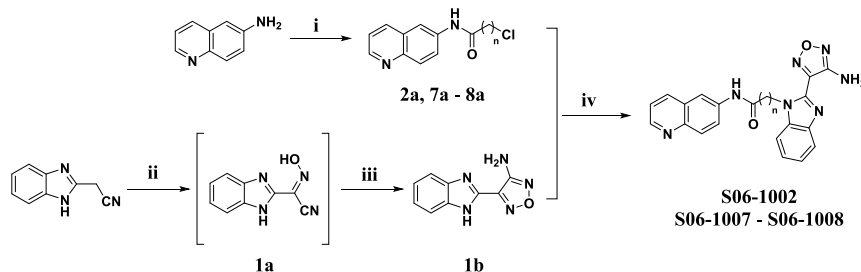
[a]Reagents and conditions: (i) chloroacetyl chloride (or 3-chloropropionyl chloride or 5-chlorovaleryl chloride), NaHCO$_3$, chloroform, r.t., 2 h; (ii) NaNO$_2$, AcOH, 0 °C, 0.5 h; (iii) NH$_2$OH HCl, KOH, (MeOCH$_2$CH$_2$)$_2$O, 110 °C, 6 h; (iv) Cs$_2$CO$_3$, dimethylformamide (DMF), 70 °C, 7 h.

Scheme 2. General Procedure for the Preparation of Terminal Compounds S06-1003 to S06-1006[a]
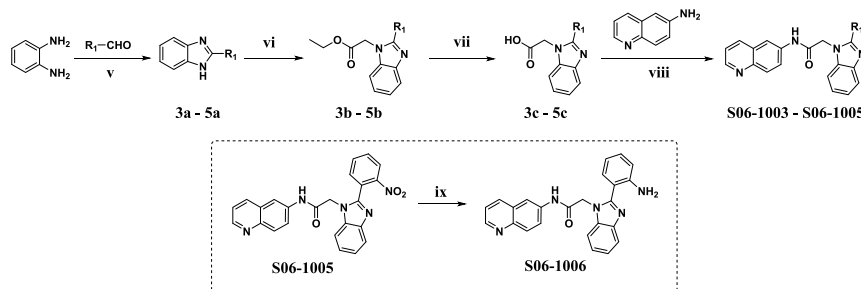
[a]Reagents and conditions: (v) NaHSO$_3$, DMF, 80 °C, 5 h; (vi) BrCH$_2$COOEt, MeCN, Cs$_2$CO$_3$, r.t., 30 min; (vii) 1 N LiOH H$_2$O, tetrahydrofuran (THF)/MeOH, r.t., 12 h; (viii) HATU, DIEA, DMF, r.t., 12 h; (ix) 10% Pd/C, N$_2$H$_4$ H$_2$O, THF, reflux, 5 h.

To confirm the importance of the large polyaromatic Moiety A and its nonpolar interaction with Trp82, we replaced the oxadiazole ring with other aromatic rings, such as furan and phenyl rings. Following Schemes 1 and 2, we synthesized compounds S06-1002 to S06-1006. The synthetic route for S06-1002 was initiated from commercially available 6-amino-quinoline, which reacted with chloroacetyl chloride to afford 2a. The commercially available reactant (2-benzimidazolyl)-acetonitrile was mixed with NaNO$_2$ in acetic acid as a solvent to produce the transitional intermediate 1a, which was subsequently reacted with hydroxylamine hydrochloride to afford 1b. Terminal compounds S06-1002 were obtained with 1b and 2a as reactants at the temperature of 70 °C. For compounds S06-1003 to S06-1005, the synthetic procedure was initiated using o-phenylenediamine, which reacted with aromatic aldehyde to afford intermediates 3a−5a. These intermediates reacted with ethyl bromoacetate to produce compounds 3b−5b, followed by hydrolysis to obtain 3c−5c. Finally, terminal compounds were produced by amidation with 6-aminoquinoline, using HATU as a condensation agent and N,N-diisopropylethylamine (DIEA) as the base.
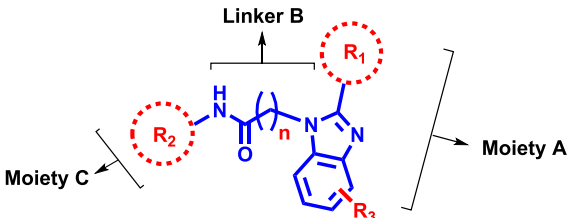
From the results obtained from the target inhibition assay of compounds S06-1002 to S06-1006 (Table 1), we found that the activity of derivative S06-1002, although slightly lower than the lead compound, was basically maintained. However, after replacing the oxadiazole ring with other aromatic rings, such as furan and benzene, the inhibitory ability of compounds S06-1003 and S06-1004 obviously declined. Moreover, we synthesized S06-1005 containing a 2-nitrobenzene ring and S06-1006 containing a 2-aminobenzene ring to mimic the primary amino group on oxadiazole and the large polyaromatic-ring structure; however, these two compounds still presented poor BChE inhibitory activity. We conducted a three-dimensional configuration simulation to explain this phenomenon, and

the results are shown in Figure 2. The amino-oxadiazole moiety is a prerequisite for the formation of the "tetraaromatic ring" planar structure. Replacement with other ring systems was unable to constitute the large planar system due to the deviation of the dihedral angle, further leading to the complete loss of inhibitory activity.

The tetracyclic system is a prerequisite for high enzyme inhibitory activity, while the insertion of Moiety C into the subpocket at the bottom of the gorge is presumed to be the key to exerting high selectivity toward BChE against AChE. Therefore, we fixed the oxadiazole ring at Moiety A and synthesized S06-1007 and S06-1008 (Scheme 1) to explore the effect of Linker B on inhibitory activity. The synthesis of S06-1007 and S06-1008 was similar to that of S06-1002, using 3-chloropropionyl chloride or 5-chlorovaleryl chloride to replace chloroacetyl chloride to afford a longer linker. The other reagents and conditions were conventional.

From the results given in Table 1, when the length of the linker was slightly increased, the activity of the compounds was enhanced accordingly. However, excessively long chains led to a loss of inhibitory capacity. According to Figure 1C, we speculated that a moderate length of the linker possibly facilitated deep insertion of Moiety C into the subpocket; however, excessive length resulted in a certain hindrance, leading to the loss of activity (S06-1008). From this point of view, we could infer that the pocket occupied by Moiety C also needed to be carefully considered during the structural modification process, as we found that the inhibitory ability of compound S06-1002 was slightly lower than that of the lead compound. Introducing proper substituents to Moiety C may improve the activity.

To explore the structure−activity relationship (SAR) of Moiety C and the volume of the pocket it occupies, we designed and synthesized 34 derivatives, replacing the quinoline ring with

Table 1. BChE Inhibition of Compounds S06-1002 to S06-1045[a,b,c]

Cpd.	n	R_1	R_2	R_3	eqBChE (IC$_{50}$, μM)	hBChE (IC$_{50}$, μM)
S06-1001	1	4-amino-furazan-3-yl	2-methylquinolin-6-yl	H	0.177 ± 0.029	0.322 ± 0.073
S06-1002	1	4-amino-furazan-3-yl	quinoline-6-yl	H	0.705 ± 0.213	n. d.
S06-1003	1	furan-3-yl	quinoline-6-yl	H	n. a.	n. d.
S06-1004	1	phenyl	quinoline-6-yl	H	n. a.	n. d.
S06-1005	1	2-nitrophenyl	quinoline-6-yl	H	n. a.	n. d.
S06-1006	1	2-aminophenyl	quinoline-6-yl	H	n. a.	n. d.
S06-1007	2	4-amino-furazan-3-yl	quinoline-6-yl	H	0.253 ± 0.105	n. d.
S06-1008	4	4-amino-furazan-3-yl	quinoline-6-yl	H	n. a.	n. d.
S06-1009	1	4-amino-furazan-3-yl	quinoline-5-yl	H	0.920 ± 0.336	n. d.
S06-1010	1	4-amino-furazan-3-yl	quinoline-4-yl	H	0.051 ± 0.010	0.212 ± 0.059
S06-1011	1	4-amino-furazan-3-yl	quinoline-3-yl	H	0.020 ± 0.006	0.016 ± 0.004
S06-1012	1	4-amino-furazan-3-yl	quinoline-2-yl	H	0.507 ± 0.132	n. d.
S06-1013	1	4-amino-furazan-3-yl	naphthalen-2-yl	H	0.352 ± 0.180	n. d.
S06-1014	1	4-amino-furazan-3-yl	naphthalen-1-yl	H	0.044 ± 0.013	0.022 ± 0.011
S06-1015	1	4-amino-furazan-3-yl	4-bromonaphthalen-1-yl	H	0.006 ± 0.003	0.032 ± 0.016
S06-1016	1	4-amino-furazan-3-yl	phenyl	H	2.960 ± 0.438	n. d.
S06-1017	1	4-amino-furazan-3-yl	2-fluorophenyl	H	0.124 ± 0.041	n. d.
S06-1018	1	4-amino-furazan-3-yl	3-fluorophenyl	H	1.043 ± 0.319	n. d.
S06-1019	1	4-amino-furazan-3-yl	2,3-difluorophenyl	H	0.270 ± 0.090	n. d.
S06-1020	1	4-amino-furazan-3-yl	2-chlorophenyl	H	2.732 ± 1.297	n. d.
S06-1021	1	4-amino-furazan-3-yl	3-chlorophenyl	H	0.033 ± 0.012	0.128 ± 0.060
S06-1022	1	4-amino-furazan-3-yl	4-chlorophenyl	H	n. a.	n. d.
S06-1023	1	4-amino-furazan-3-yl	3-bromophenyl	H	0.083 ± 0.022	0.212 ± 0.086
S06-1024	1	4-amino-furazan-3-yl	4-bromophenyl	H	n. a.	n. d.
S06-1025	1	4-amino-furazan-3-yl	3-methylphenyl	H	0.236 ± 0.059	n. d.
S06-1026	1	4-amino-furazan-3-yl	4-methylphenyl	H	10.290 ± 8.231	n. d.
S06-1027	1	4-amino-furazan-3-yl	2,3-dimethylphenyl	H	0.326 ± 0.075	n. d.
S06-1028	1	4-amino-furazan-3-yl	3-methoxyphenyl	H	1.711 ± 0.735	n. d.
S06-1029	1	4-amino-furazan-3-yl	4-methoxyphenyl	H	n. a.	n. d.
S06-1030	1	4-amino-furazan-3-yl	2,3,4-trimethoxyphenyl	H	6.643 ± 2.276	n. d.
S06-1031	1	4-amino-furazan-3-yl	3-nitrophenyl	H	0.031 ± 0.003	0.025 ± 0.009
S06-1032	1	4-amino-furazan-3-yl	4-nitrophenyl	H	0.030 ± 0.007	0.080 ± 0.031
S06-1033	1	4-amino-furazan-3-yl	4-aminophenyl	H	n. a.	n. d.
S06-1034	1	4-amino-furazan-3-yl	3-cyanophenyl	H	0.051 ± 0.012	0.250 ± 0.088
S06-1035	1	4-amino-furazan-3-yl	3-acetylphenyl	H	0.191 ± 0.048	n. d.
S06-1036	1	4-amino-furazan-3-yl	4-acetylphenyl	H	2.267 ± 0.216	n. d.
S06-1037	1	4-amino-furazan-3-yl	3- methoxycarbonyl	H	0.027 ± 0.013	0.180 ± 0.056
S06-1038	1	4-amino-furazan-3-yl	4- methoxycarbonyl	H	5.376 ± 0.816	n. d.
S06-1039	1	4-amino-furazan-3-yl	3-acetamidophenyl	H	1.125 ± 0.493	n. d.
S06-1040	1	4-amino-furazan-3-yl	4-acetamidophenyl	H	6.538 ± 1.220	n. d.
S06-1041	1	4-amino-furazan-3-yl	biphenyl	H	n. a.	n. d.
S06-1042	1	4-amino-furazan-3-yl	benzo[1,3]dioxol-5-yl	H	2.206 ± 1.133	n. d.
S06-1043	1	4-amino-furazan-3-yl	quinoline-6-yl	5,6-dimethyl	11.25 ± 10.03	n. d.
S06-1044	1	4-amino-furazan-3-yl	quinoline-3-yl	5,6-dimethyl	28.53 ± 56.50	n. d.
S06-1045	1	4-amino-furazan-3-yl	naphthalen-1-yl	5,6-dimethyl	0.108 ± 0.037	n. d.
Tacrine					0.005 ± 0.001	n. d.

[a]n. d., not determined. [b]n. a., no activity for their inhibitory rates less than 50% at a concentration of 10 μM. Detailed inhibitory rates (IRs) are summarized in the Supporting Information, Figure S2. [c]All tests are expressed as the mean ± standard error of the mean (SEM) of three independent experiments.

diverse aromatic rings and fixing Linker B to n = 1, following Scheme 3. The synthetic route was similar to that of **S06-1002**

and initiated using diverse commercially available amines, which reacted with chloroacetyl chloride to afford **9a** to **42a**. The other
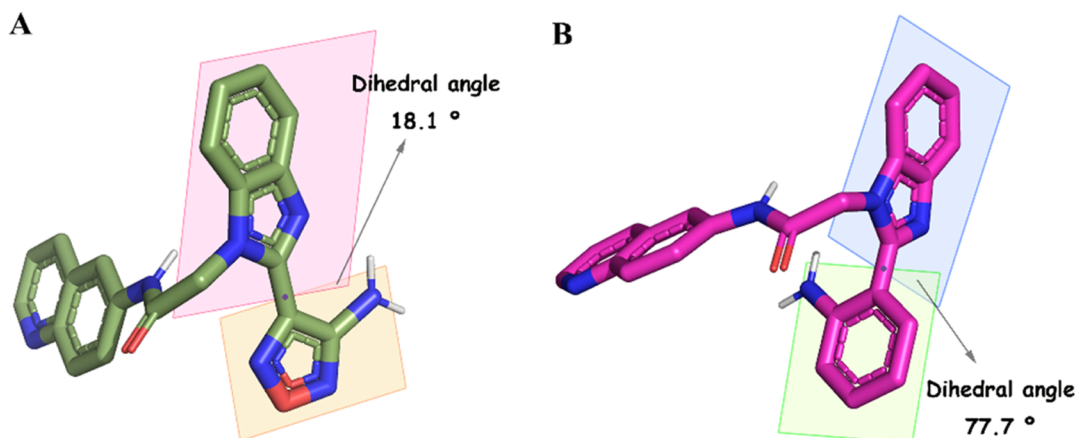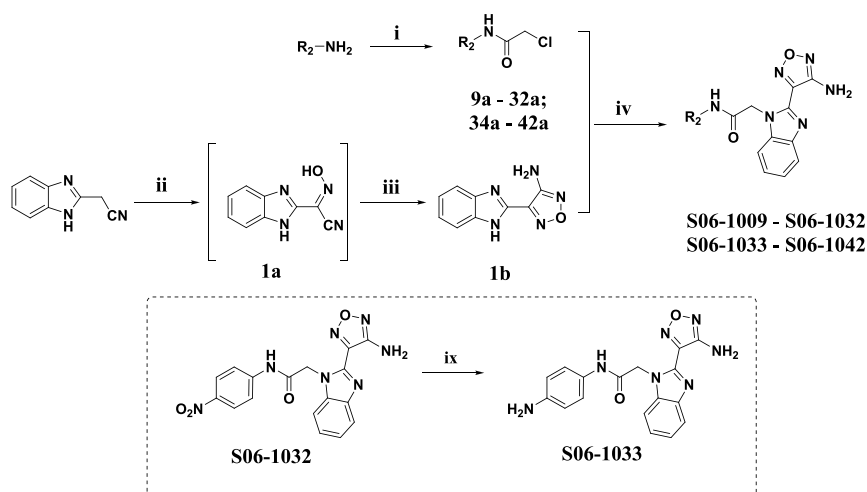
Figure 2. Three-dimensional configuration simulation of **S06-1002** and **S06-1006**.

Scheme 3. General Procedure for the Preparation of Terminal Compounds S06-1009 to S06-1042[a]

[a]Reagents and conditions: (i) chloroacetyl chloride, NaHCO$_3$, chloroform, r.t., 2 h; (ii) NaNO$_2$, AcOH, 0 °C, 0.5 h; (iii) NH$_2$OH HCl, KOH, (MeOCH$_2$CH$_2$)$_2$O, 110 °C, 6 h; (iv) Cs$_2$CO$_3$, DMF, 70 °C, 7 h; (ix) 10% Pd/C, N$_2$H$_4$ H$_2$O, THF, reflux, 5 h.

Scheme 4. General Procedure for the Preparation of Terminal Compounds S06-1043 to S06-1045[a]
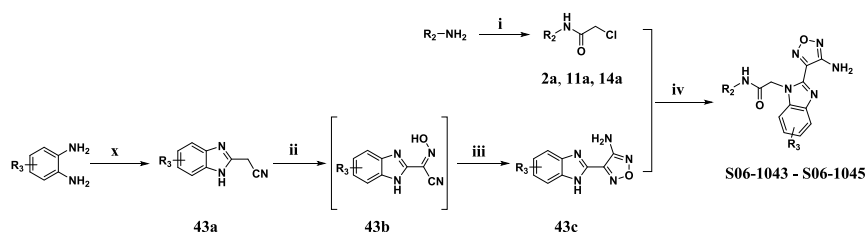

[a]Reagents and conditions: (i) chloroacetyl chloride, NaHCO$_3$, chloroform, r.t., 2 h; (ii) NaNO$_2$, AcOH, 0 °C, 0.5 h; (iii) NH$_2$OH HCl, KOH, (MeOCH$_2$CH$_2$)$_2$O, 110 °C, 6 h; (iv) Cs$_2$CO$_3$, DMF, 70 °C, 7 h; (x) ethyl cyanoacetate, 185 °C, under argon, 2 h.

reagents and conditions were the same as those used for **S06-1002**.

As shown in Table 1, derivatives containing a bicyclic substitution at Moiety C commonly possessed good BChE inhibitory capacities. In particular, compounds **S06-1011**, **S06-1014**, and **S06-1015** presented nanomolar inhibition against *eq*BChE and *h*BChE. Derivatives **S06-1016** to **S06-1042** containing a benzene ring or a substituted benzene ring at Moiety C displayed greatly varied capacities. Inhibitors with substituents in the meta position showed preferable potency with an IC$_{50}$ value range of 27–1711 nM and a selectivity against

BChE that was even higher than 3000-fold (Supporting Information, Figure S2). However, compounds containing non-, ortho-, and para-substituted benzenes showed reduced inhibitory capacity. In particular, compounds containing *p*-substituted benzene rings, except for **S06-1032** (*eq*BChE IC$_{50}$ = 0.030 ± 0.007 μM), commonly lost their inhibitory activities completely. Although several *meta*-substituted benzene-containing inhibitors have comparable activity to compounds containing bicyclic rings, they have much higher ligand efficiency (LE), which is important for druggability. Due to their excellent inhibitory activity against *eq*BChE, compounds
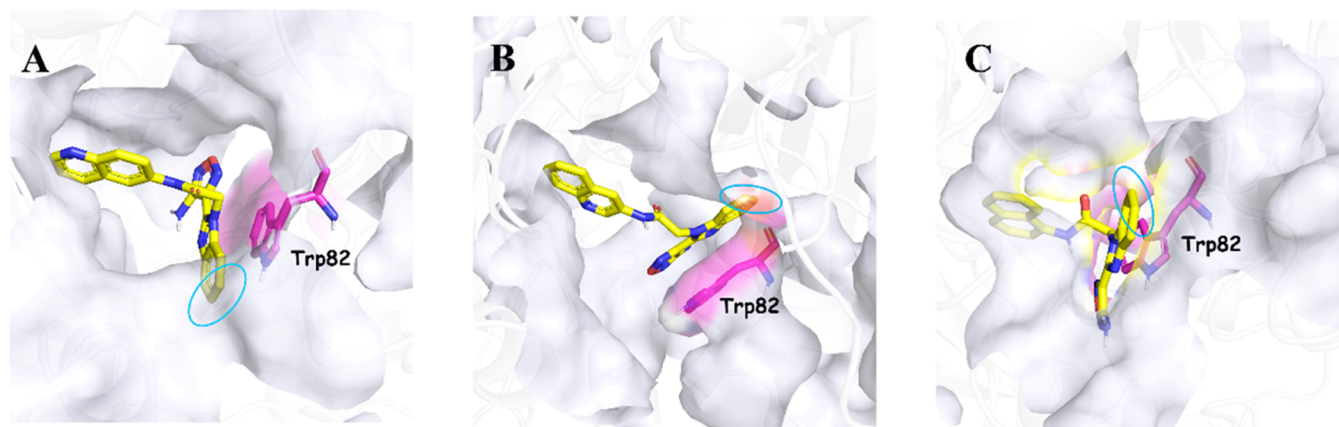
Figure 3. MD results of compounds **S06-1002** (A), **S06-1011** (B), and **S06-1014** (C). 5,6-Position of the benzimidazole has been marked by a blue circle (PDB code: 5k5e).

Table 2. *In Vitro* Potential Cytotoxicity on Neurocytes and Hepatocytes[a,d]

Cpd.	SH-SY5Y $IC_{50}, \mu M$ (SR, %)	PC12 $IC_{50}, \mu M$ (SR, %)	BV2 $IC_{50}, \mu M$ (SR, %)	HepG2 $IC_{50}, \mu M$ (SR, %)	L02 $IC_{50}, \mu M$ (SR, %)
S06-1001	35.10 ± 40.22	91.50 ± 10.50	59.79%[c]	17.28 ± 9.70	61.49%[c]
S06-1011	62.19%[c]	33.45 ± 9.90	69.72%[c]	84.31 ± 22.8	70.64%[c]
S06-1014	40.84%[b]	44.44%[b]	82.90%[c]	5.05 ± 1.24	73.52%[c]
S06-1015	62.37%[c]	52.21%[c]	55.66%[c]	73.24%[c]	86.55%[c]
S06-1031	82.67%[c]	58.34%[c]	94.23%[c]	75.46%[c]	87.01%[c]

[a]SR, survival rate at [b]2.5 μM or [c]100 μM. [d]All tests were expressed as the mean $\pm$ SEM of three independent experiments.

with IC_{50} values less than 100 nM against *eq*BChE were subsequently evaluated for their inhibition against *h*BChE (Table 1). As a result, four compounds, namely, **S06-1011**, **S06-1014**, **S06-1015**, and **S06-1031**, exhibited target inhibition values of less than 50 nM.

Finally, to explore the possibility of introducing substituents on benzimidazole, we fixed Moiety C as bicyclic rings (quinoline or naphthalene ring) and synthesized compounds **S06-1043** to **S06-1045** following the procedure shown in Scheme 4. Due to the commercial unavailability of substituted (2-benzimidazolyl)-acetonitrile, we synthesized **43a** with substituted 1,2-diaminobenzene and ethyl cyanoacetate as reactants. **43a** reacted with sodium nitrite and then hydroxylamine hydrochloride to afford **43c**. Terminal compounds **S06-1043** to **S06-1045** were finally provided with **43c** and **2a**, **11a**, or **14a**.

From the results in Table 1, compounds containing substituents on benzimidazole presented different inhibitory activities due to the difference in Moiety C. The structures of Moiety C could lead to variation in the orientation of the overall configuration. We subsequently conducted molecular docking (Supporting Information, Figure S3) and MD simulations (Figure 3, Supporting Information, Figure S4) to explain this phenomenon. Although all of the polyaromatic moieties (Moiety A) formed $\pi-\pi$ interactions with Trp82, the overall compounds displayed diverse orientations induced by single-bond rotation. When Moiety C was fixed as a naphthalene ring (compound **S06-1014**), the 5,6-position of the benzimidazole faced the solvent region, and its substitution exerted little effect on the activity. However, other structures of Moiety C can cause the 5,6-position of the benzimidazole to insert itself into a subpocket (Figure 3A,B). Certain steric hindrances led to a great decrease and loss of the BChE-inhibiting ability. Based on these

findings, structural modification of the benzimidazole is not preferred.

After four rounds of structural modification and SAR discussion, four compounds, namely, **S06-1011**, **S06-1014**, **S06-1015**, and **S06-1031** with high activity and supreme selectivity regarding the target level, were concluded to be representative BChE inhibitors for further evaluation of safety and efficacy *in vitro* and *in vivo*.

2.2. Safety Investigations. *In vitro* potential cytotoxicity of lead and active compounds was evaluated through the 3-(4,5-dimethylthiazol-2-yl)-2,5-diphenyltetrazolium (MTT) assay on diverse types of neurocytes, PC12, SH-SY5Y, and BV2 cell lines.[42] Except for **S06-1014**, which was toxic to PC12 (40.84% cell viability under 2.5 μM) and SH-SY5Y (44.44% cell viability under 2.5 μM) cell lines, most of the active compounds were proven to lead to weak or no toxicity (Table 2). These results indicated that three active compounds (**S06-1011**, **S06-1015**, and **S06-1031**) exhibited sufficient *in vitro* neurosafety and could be further tested for their neuroprotective effects.

Subsequently, acute toxicity tests for active compounds **S06-1011**, **S06-1015**, and **S06-1031** were carried out in healthy ICR mice at the single-dose level. No death occurred after intragastric administration of compounds even at a relatively high dose of 1 g/kg. Mice in the drug administration groups (male and female) grew normally. The body weights of the mice gradually increased (Figure 4A), and no significant behavioral abnormalities were observed over the 14 day period.

The toxicity to the liver was evaluated by monitoring *in vitro* antiproliferative effects against hepatocytes (Table 2), the levels of aspartate aminotransferase (AST) and alanine aminotransferase (ALT) (Figure 4B), and hematoxylin−eosin (HE) staining (Figure 4C). Except for **S06-1014**, compounds
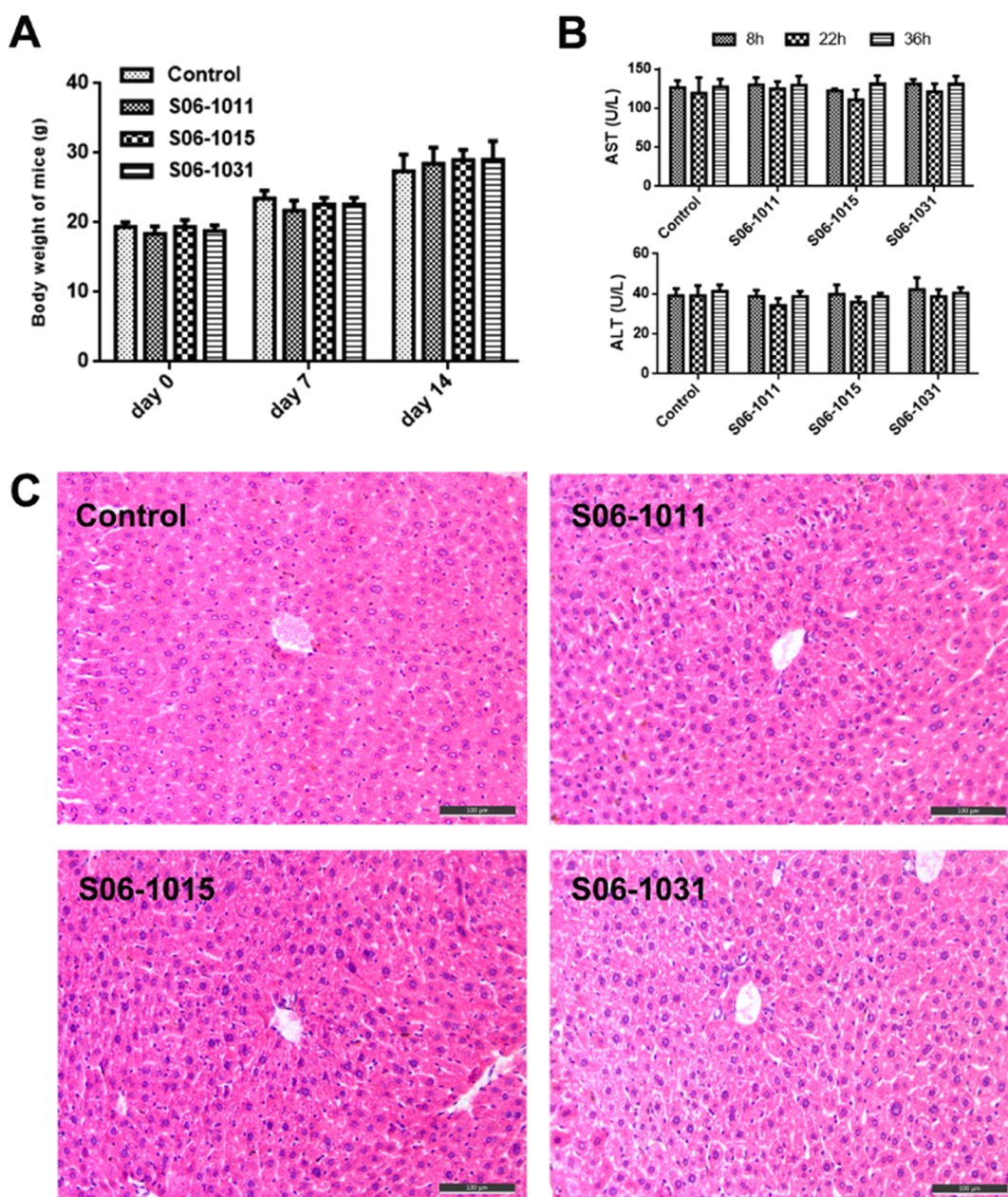
Figure 4. (A) Body weight of ICR mice (g)-time (day). (B) Aspartate aminotransferase (AST) and alanine aminotransferase (ALT) activities at time points (8, 22, and 36 h) after the administration of vehicle only (blank control) or compounds **S06-1011**, **S06-1015**, and **S06-1031**. (C) Histomorphological appearances of the liver of male mice after treatment with the vehicle only (blank control) or 22 h after administration of compounds **S06-1011**, **S06-1015**, and **S06-1031**. Hematoxylin−eosin (HE) staining, original magnification ×100.

presented weak cytotoxicity against HepG2 or L02 cell lines. Due to toxicity to some cell lines, **S06-1014** was no longer used as a representative for further studies. To ensure the hepatic safety of **S06-1011**, **S06-1015**, and **S06-1031**, we next investigated drug-induced hepatotoxicity. Heparinized serum was collected at different time points (8, 22, and 36 h) after the administration of normal saline (as a control) or compounds **S06-1011**, **S06-1015**, and **S06-1031**. Compared to the blank-control group, the three compounds did not show any remarkable damage at any of the time points. Afterward, morphological studies by immunohistochemical staining were applied to assess the hepatotoxicities of **S06-1011**, **S06-1015**, and **S06-1031**. Treatment with **S06-1011**, **S06-1015**, or **S06-1031** did not present obvious morphological changes in the liver

compared to the control group. Taken together, all three compounds exhibited high safety for the center and periphery.

2.3. PK Evaluation and BBB Penetration. The metabolic stabilities in the liver microsomes of **S06-1011**, **S06-1015**, and **S06-1031** were evaluated using the long-acting drug ketanserin as a reference control. As expected, all three compounds were stable in the presence of human liver microsomes (Figure 5A,B). The intrinsic human microsome clearances for the active compounds **S06-1011**, **S06-1015**, and **S06-1031** were lower than that for the positive control ketanserin, showing longer half-lives. Furthermore, compound **S06-1011** with the longest $T_{1/2}$ in human liver microsomes was selected for *in vitro* metabolic pathway analysis and *in vivo* pharmacokinetic (PK) evaluation. After compound **S06-1011** was incubated with liver microsomes *in vitro*, two possible forms of metabolites were identified in the
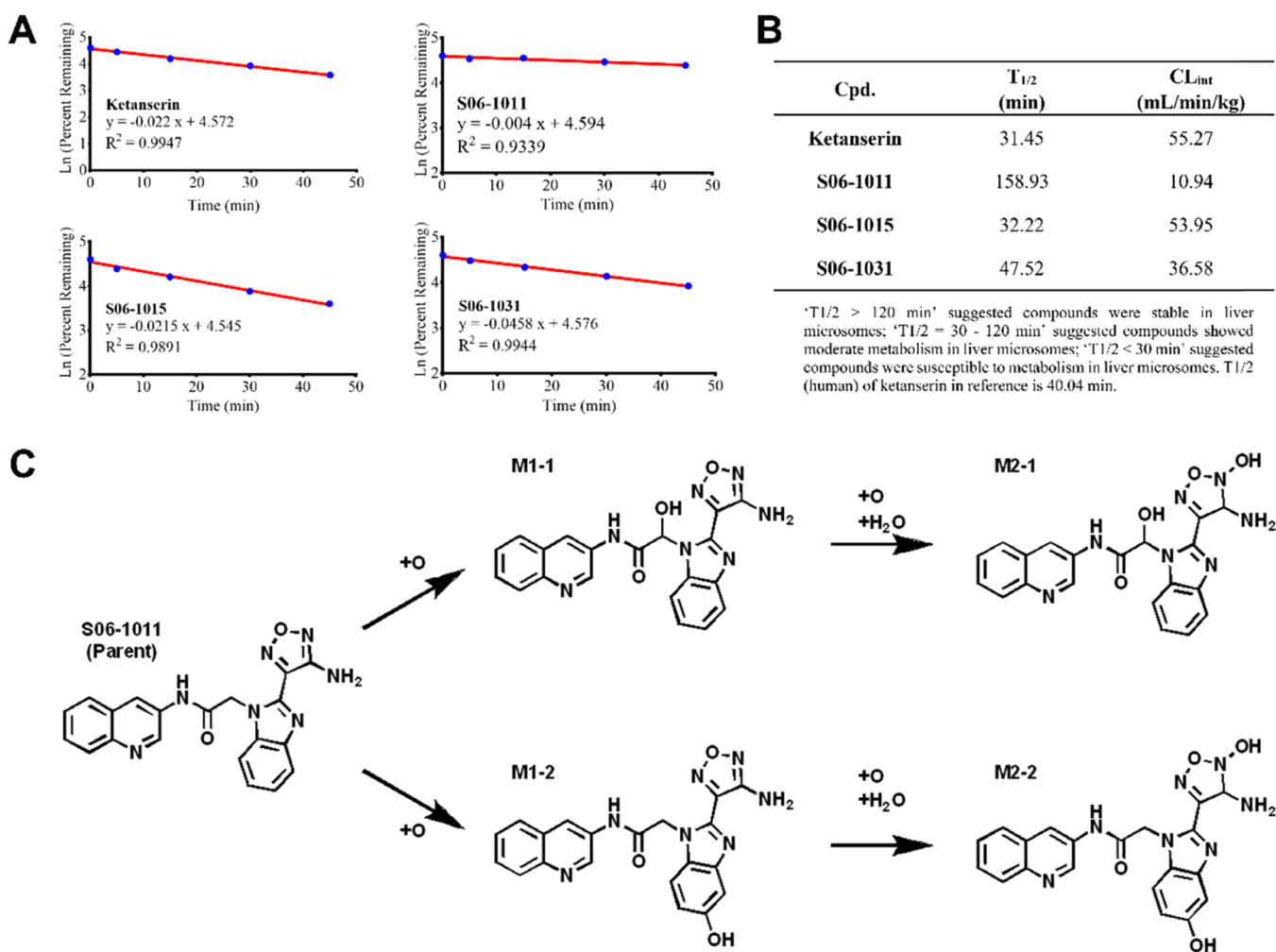
Figure 5. Human liver microsomal stability and metabolite analysis. (A) Percentage of remaining compounds at different time points. (B) Parameters of liver microsomal stability. All data are the mean value of two independent experiments. (C) Possible biotransformation pathway of the compound **S06-1011** in the liver.

samples: mono-oxidation metabolites and double-oxidation metabolites. The identification information is shown in Table S1 (Supporting Information), and the metabolic pathway is presented in Figure 5C. The metabolites all retain the pivotal four-ring skeleton of benzimidazole-oxadiazole. Hence, we considered that **S06-1011** could exert its pharmacological effects for an extended time.

The PK profiles (Table 3) in the male SD rat model showed that compound **S06-1011** was slowly absorbed with a T_{max} value of 9.5 h and a favorable half-life of 5.47 h following a single-dose oral administration (10 mg/kg). Notably, compound **S06-1011** enters the enterohepatic circulation (Supporting Information, Figure S5), which means that it is excreted into the intestine via bile and reabsorbed in the intestine. The overall PK property of compound **S06-1011** was desirable, as approved by its high bioavailability (F_{oral} = 73.37 ± 0.06%). The results indicated that compound **S06-1011** was a potential drug candidate and provided a solid basis for the further evaluation of *in vitro* and *in vivo* biological activities.

As compounds were exploited for treating neurodegenerative diseases, we performed a parallel artificial membrane permeation assay of the blood−brain barrier (PAMPA−BBB) to assay the BBB penetration potential of compounds **S06-1011**, **S06-1015**, and **S06-1031**.[43] According to the tested permeability (Figure 6,
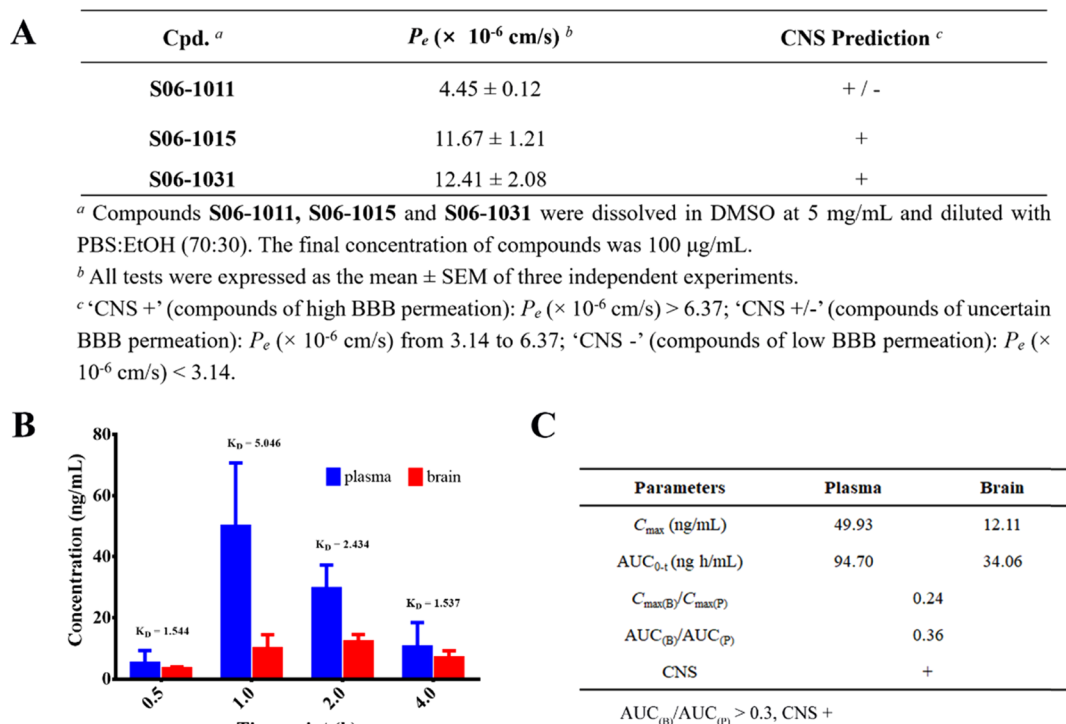
Table 3. SD Rat PK Profiles of Compound S06-1011

parameter[a]	10 mg/kg (p.o.)	10 mg/kg (i.v.)
AUC_{0-t} (ng h/mL)	627.52 ± 45.35	859.64 ± 81.54
AUC_{0-inf} (ng h/mL)	661.74 ± 65.66	1092.11 ± 307.19
MRT_{inf} (h)	11.56 ± 1.89	14.14 ± 12.26
$t_{1/2}$ (h)	5.47 ± 1.59	8.87 ± 11.09
T_{max} (h)	9.50 ± 2.07	0.017 ± 0.00
C_{max} (ng/mL)	44.73 ± 3.40	488.33 ± 32.32
F (%)		73.37 ± 0.06%

[a]PK parameters in Sprague−Dawley rats (male). All data are the mean ± SD of eight independent experiments. Abbreviations: AUC, area under the concentration−time curve; MRT, mean residence time; $t_{1/2}$, time required for the concentration to diminish by a half; T_{max}, time to reach C_{max}; C_{max}, peak plasma concentration of a drug after administration.

Supporting Information, Figure S6), compounds **S06-1015** and **S06-1031** presented a possibility for BBB penetration *in vitro*, while it was uncertain whether or not compound **S06-1011** penetrates the BBB and reached the biological targets. Hence, we assayed the brain distribution of compound **S06-1011** in mice. The results (Figure 6) showed that although the brain exposure was relatively low, it was stable, indicating that this compound could be stabilized in the brain to exert its efficacy. As

A

Cpd. [a]	P_e (× 10^{-6} cm/s) [b]	CNS Prediction [c]
S06-1011	4.45 ± 0.12	+ / -
S06-1015	11.67 ± 1.21	+
S06-1031	12.41 ± 2.08	+

[a] Compounds **S06-1011**, **S06-1015** and **S06-1031** were dissolved in DMSO at 5 mg/mL and diluted with PBS:EtOH (70:30). The final concentration of compounds was 100 µg/mL.

[b] All tests were expressed as the mean ± SEM of three independent experiments.

[c] 'CNS +' (compounds of high BBB permeation): P_e (× 10^{-6} cm/s) > 6.37; 'CNS +/-' (compounds of uncertain BBB permeation): P_e (× 10^{-6} cm/s) from 3.14 to 6.37; 'CNS -' (compounds of low BBB permeation): P_e (× 10^{-6} cm/s) < 3.14.

B

C

Parameters	Plasma	Brain
C_{max} (ng/mL)	49.93	12.11
AUC_{0-t} (ng h/mL)	94.70	34.06
$C_{max(B)}/C_{max(P)}$		0.24
$AUC_{(B)}/AUC_{(P)}$		0.36
CNS		+

$AUC_{(B)}/AUC_{(P)}$ > 0.3, CNS +

Figure 6. (A) PAMPA−BBB assay results and predicted penetration of active compounds **S06-1011**, **S06-1015**, and **S06-1031** in the CNS. (B) BBB exposure at several time points after oral administration of **S06-1011**. K_D, ratio of plasma exposure to brain exposure. (C) Parameters of tissue distribution. Abbreviations: C_{max}, peak exposure of **S06-1011** after administration; AUC, area under the concentration−time curve.

calculated by $AUC_{(B)}$ vs $AUC_{(P)}$, **S06-1011** was able to partially penetrate the BBB and enter the CNS.

2.4. *In Vitro* Neuroprotection in SH-SY5Y Cells. Neuroprotection by combating oxidative stress has long been identified to be an important strategy for AD treatment.[44] Hence, we next evaluated the cytoprotective effects of optimal compounds against H_2O_2-, glutamate-, and $A\beta_{1-42}$-induced cell damage with the methyl thiazolyl tetrazolium (MTT) assay in SH-SY5Y cells, three well-established cellular models of neurodegenerative disorders.[45−47] The addition of H_2O_2 (200 µM) to the growth media caused significant cell death by reducing the cell viability (62.36%). To assess the neuroprotective potential of the test compounds, cells were pretreated for 2 h with compounds **S06-1011**, **S06-1015**, and **S06-1031** (2.5 and 10 µM) prior to H_2O_2 insult for 24 h. As shown in Figure 7A, the selected derivatives **S06-1011** and **S06-1031** exhibited pronounced neuroprotective effects at concentrations of 2.5 and 10 µM in a dose-dependent manner.

Glutamate excitotoxicity is responsible for the pathology of chronic disorders. Exposure to glutamate results in lowered glutathione levels, leading to oxidative stress and cell death. As shown in Figure 7B, the addition of glutamate (20 mM) elicited a significant decline in cell viability (∼50%) compared to the control. Preincubation with compounds **S06-1011** and **S06-1031** moderately rescued SH-SY5Y cells insulted by glutamate at a concentration of 10 µM.

The $A\beta$ hypothesis has increasingly been proven to play a pivotal role in AD pathology.[48] Abnormal $A\beta$ plaques can induce a series of nerve injuries. It has been reported that $A\beta$ aggregation is related to the production of reactive oxygen species (ROS), mitochondrial dysfunction, local microglial activation, cytokine release, and multiprotein inflammation, which are all harmful for central function.[49−52] To compare

neuronal death induced by $A\beta_{1-42}$ in the absence or presence of diverse concentrations of compounds **S06-1011**, **S06-1015**, and **S06-1031**, an MTT assay was performed. As exhibited in Figure 7C, incubation of SH-SY5Y cells with 15 µM $A\beta_{1-42}$ caused pronounced cytotoxicity. To our delight, compounds **S06-1011** and **S06-1031** exhibited remarkable neuroprotective effects at a relatively low concentration of 2.5 µM. All three representative compounds presented concentration-dependent neuroprotective properties. Notably, at 10 µM, compound **S06-1031** almost protected SH-SY5Y cells from $A\beta_{1-42}$ peptide toxicity.

ROS are a series of biological molecules produced by aerobic organisms that maintain equilibrium and are important in normal cell signaling under physiological conditions.[44,53] However, it has been observed that the antioxidant mechanism balance in the postmortem brains of AD patients could be interrupted by aberrantly increased ROS levels. Hence, we assessed the preliminary anti-inflammatory profiles of the best molecules, namely, **S06-1011**, **S06-1015**, and **S06-1031**, by examining the level of released ROS in the mouse neuroglial BV2 cell line. A BV2 cell model with high ROS release stimulated by lipopolysaccharides (LPS) (2.5 µg/mL) was established.[54] Compounds **S06-1011**, **S06-1015**, and **S06-1031** were evaluated to pronouncedly hinder the increase of LPS-induced ROS production without affecting the morphology of BV2 cells, indicating their abilities to reduce oxidative stress (Figure 7D, Supporting Information, Figure S7). The ROS reduction capacities of **S06-1011** and **S06-1031** were better than that of the lead compound **S06-1001**.

2.5. *In Vivo* Behavioral Assays. To determine whether treatment with the representative compound **S06-1011**, **S06-1015**, or **S06-1031** could improve scopolamine-induced acute memory impairment, we performed the Morris water maze test, which has been extensively used to evaluate potential
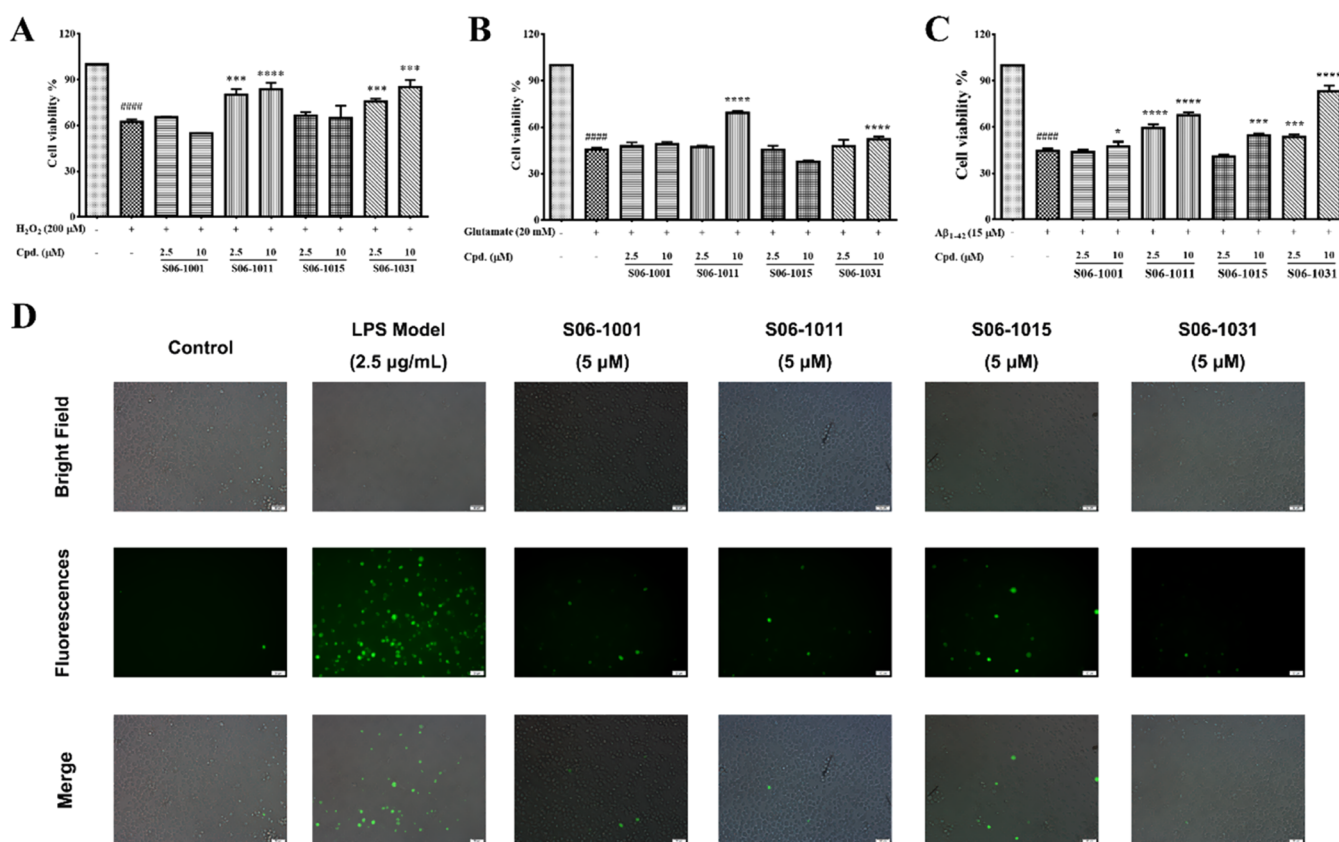
Figure 7. (A−C) Neuroprotective effects of compounds **S06-1001**, **S06-1011**, **S06-1015**, and **S06-1031** against H_2O_2-, glutamate- and $A\beta_{1-42}$-induced cell insults on the SH-SY5Y cell line. SH-SY5Y cells were preincubated with 2.5 and 10 μM of the test compounds (**S06-1011**, **S06-1015**, and **S06-1031**) for 2 h and subsequently exposed to H_2O_2 (200 μM) (A), glutamate (20 mM) (B), or $A\beta_{1-42}$ (15 μM) (C) for 24 h. The cell viability was measured using an MTT assay. The data are expressed as mean $\pm$ SEM of three independent experiments ($^{####}p < 0.0001$ vs the control group; $^*p < 0.05$, $^{***}p < 0.001$, $^{****}p < 0.0001$ vs the model group). (D) Detection of reactive oxygen species (ROS) production in BV2 cells using fluorescence microscopy analysis. The amount of intracellular ROS production was expressed by green fluorescence intensity (GFI). To avoid errors in the fluorescence brightness, the exposure time was fixed at 10.2 ms.
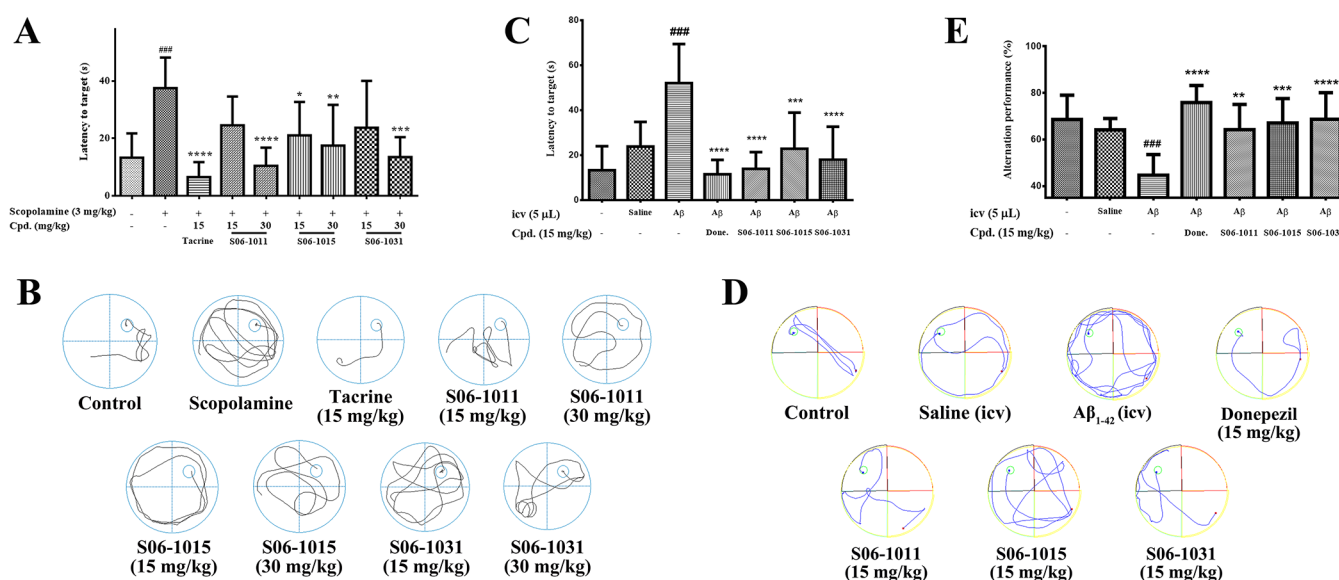
Figure 8. (A, B) Effects of compounds on scopolamine-induced AD-like cognitive deficits in ICR mice. (A) Escape latency to the platform in Morris water maze. (B) Average tracks of mice in Morris water maze. Data are presented as the mean $\pm$ SD ($n = 8$; $^{###}p < 0.001$ vs the control group; $^*p < 0.05$, $^{**}p < 0.01$, $^{***}p < 0.001$, $^{****}p < 0.0001$ vs the scopolamine model group). (C−E) Effects of compounds on $A\beta_{1-42}$ peptide-induced AD-like cognitive deficits in ICR mice. (C) Escape latency to the platform in the Morris water maze. (D) Average tracks of mice in the Morris water maze. (E) Spontaneous alternation performances in the Y maze test. Data are presented as the mean $\pm$ SD ($n = 8$; $^{##}p < 0.01$, $^{###}p < 0.001$ vs the sham-operation group; $^{**}p < 0.01$, $^{***}p < 0.001$, $^{****}p < 0.0001$ vs the model group).
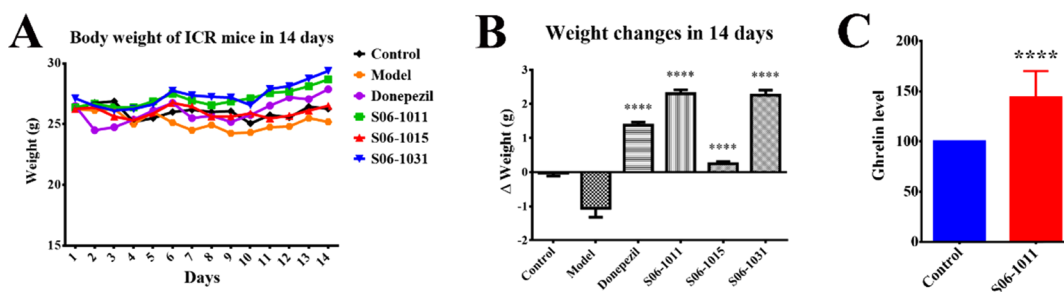
Figure 9. (A) Everyday body weight of ICR mice in 14 days. Data are presented as the mean ($n = 8$). (B) Body-weight changes in 14 days. Data are presented as the mean $\pm$ SD ($n = 8$; ****$p < 0.0001$ vs the Aβ_{1-42} model group). (C) Ghrelin level in mice plasma. Data are presented as the mean $\pm$ SD ($n = 8$; ****$p < 0.0001$ vs the control group).

therapeutic agents for treating AD. Memory training and learning were conducted for 5 days, and a probe trial was performed on the sixth day (Supporting Information, Figure S8). The results are presented in Figure 8. Compared to the control group, the spatial memory defects for mice treated with scopolamine alone (3 mg/kg, model group) were significantly shown to have a longer latency (37.45 vs 13.30 s) and a more chaotic trajectory to the target. As a positive control group, treatment with tacrine contributed to a simplified trajectory and a shorter latency to the platform (6.48 vs 37.45 s). Furthermore, compounds **S06-1011**, **S06-1015**, and **S06-1031** significantly attenuated scopolamine-induced cognitive impairment at a dose of 30 mg/kg. Although the optimal compound **S06-1011** presented a considerably short latency to the platform and a simplified trajectory, its cognitive and memory improvement effect was still inferior to that of tacrine at a low dose (15 mg/kg).

To more closely investigate the anti-AD effects of compounds, we carried out an accepted Aβ_{1-42}-induced cognitive-impaired model.[55,56] The AD-like cognitive impairment mice model was established by intracerebroventricular (icv) injection of the oligomerized Aβ_{1-42} peptide (10 μg) on day 1 (Supporting Information, Figure S8). Meanwhile, the same volume of saline was icv-injected for the sham-operation group. Donepezil, which could inhibit the formation of Aβ deposits and attenuate neural toxicity of Aβ oligomers, contributing to cognition improvement, was taken as a positive control. Donepezil, **S06-1011**, **S06-1015**, and **S06-1031** were orally administered from days 3 to 14. Behavioral studies were conducted using a Morris water maze and a Y maze. As shown in Figure 8, no remarkable differences in cognitive and learning capacities were observed between the sham-operation group and the blank control group, in terms of indistinctive latency to target, trajectory confusion, and alternation performance. Treatment with donepezil significantly shortened the latency, simplified the tracks to the target, and improved alternation performance. Moreover, intragastric administration of compounds **S06-1011**, **S06-1015**, and **S06-1031** at an equivalent (15 mg/kg) dose to donepezil entirely prevented the impact of toxic Aβ_{1-42} oligomers. In particular, **S06-1011** presented comparable effectiveness to the positive control donepezil in the Morris water maze test, reduced the target latency (51.98 to 13.83 s), and simplified the trajectory. Compound **S06-1031** showed the most enhanced alternation performance in the Y maze test (44.64% to 68.67%).

Additionally, none of the treatments (icv for peptide or po for compounds) resulted in a great loss of mouse body weight during the therapy period, presenting good tolerability of the test compounds (Figure 9). Instead, treatments with the compounds enhanced the body weight of mice, presenting significant differences from the model group. Especially for the mice in the **S06-1011** and **S06-1031** groups, there was an obvious difference in weight gain compared with the donepezil group ($p < 0.01$). To further corroborate this phenomenon, we evaluated the plasma ghrelin levels of mice in the control and **S06-1011** groups. As a result, the ghrelin level of mice in the **S06-1011** group displayed a remarkable increase. Hence, we concluded that inhibition of BChE led to an enhanced ghrelin level, which helped improve mental mood and increase appetite. This can not only play a protective role against dementia but also exert a great influence on treatment and nursing care.

Overall, three optimal compounds showed good effects in both investigated behavioral studies, successfully improving the spatial exploration ability, cognition, and memory. Together with *in vitro* neuroprotective effects, compounds **S06-1011** and **S06-1031** were identified as effective candidates for BChE inhibition and AD treatment.

3. CONCLUSIONS

In our previous work, we disclosed a hierarchical structure-based virtual screening workflow to identify a novel potent and selective anti-BChE lead compound **S06-1001** (*eq*BChE IC$_{50}$ = 0.177 ± 0.029 μM, *h*BChE IC$_{50}$ = 0.322 ± 0.073 μM). Based on molecular binding and dynamics results, 44 derivatives were synthesized and assayed for their BChE inhibitory efficacy, among which four compounds (**S06-1011**, **S06-1014**, **S06-1015**, and **S06-1031**) showed IC$_{50}$ values lower than 50 nM against human BChE. Furthermore, compounds **S06-1011**, **S06-1015**, and **S06-1031** were noncytotoxic *in vitro* and well-tolerated *in vivo* at doses up to 1 g/kg, inducing no liver side effects. Three compounds could penetrate the BBB and take effect in the CNS. In addition, all three compounds presented considerable pharmacokinetic properties, a long $t_{1/2}$, and low liver microsome clearances. Remarkably, the long-acting compound **S06-1011** showed a high oral bioavailability (73.37%).

From the perspective of pharmacodynamics, the optimal candidate compounds **S06-1011** and **S06-1031** exhibited potent antioxidant activity and neuroprotective effects against H$_2$O$_2$-, glutamate-, and Aβ_{1-42}-mediated SH-SY5Y neurotoxicity. Moreover, three compounds reduced the production of ROS induced by LPS at a concentration of 5 μM. Notably, the BChE inhibitors **S06-1011**, **S06-1015**, and **S06-1031** were shown to improve cognitive and learning abilities in scopolamine- and Aβ_{1-42} peptide-induced cognitive deficit models. This result demonstrated that the identified BChE inhibitors not only improved memory impairments by symptomatically

rescuing the cholinergic function but also protected the neural environment from Aβ oligomers and oxidative insults, which might be a potential strategy of BChE inhibition for AD treatment. Moreover, BChE inhibition by compound administration can increase the level of blood ghrelin, contributing to a significant increase in body weight by improving appetite. This important finding also indicates that inhibiting BChE can not only improve the neurological environment and cognitive impairment but also provide great convenience for caregivers.

4. EXPERIMENTAL SECTION

4.1. Chemistry. *4.1.1. General Chemistry.* Common reagents and solvents were purchased from commercial suppliers and used without further purification. Melting points were determined on a Mel-TEMP II melting point apparatus. ^{1}H and ^{13}C NMR spectra were recorded with a Bruker Avance 300 and a 100 MHz spectrometer at 300 K, using TMS as an internal standard in dimethyl sulfoxide (DMSO)-d_6. Chemical shifts (δ) are reported in parts per million (ppm), and coupling constants (J) are reported in hertz (Hz). MS spectra were recorded on an Agilent LC-MS 6120 instrument with an electrospray ionization (ESI) mass selective detector in the positive ion mode. All reaction progresses were monitored by analytical thin-layer chromatography (TLC) on precoated silica gel GF254 plates under UV light at 254 and 365 nm or through staining with iodine. Compounds were purified with flash column chromatography using silica gel (100−300 mesh) purchased from Qingdao Haiyang Chemical Co. Ltd. (China) as the stationary phase and petroleum ether/ethyl acetate or dichloromethane (DCM)/methanol mixtures as eluent systems. Purity for final compounds (higher than 95%) was measured by high-performance liquid chromatography (HPLC) with an Agilent Technologies 1260 infinity C18 4.60 mm × 150 mm × 5 μm column, eluted with a mixture of solvent methanol/distilled water [0.1% formic acid] at the flow rate of 1.0 mL/min.

4.1.2. General Synthetic Procedure for Compounds S06-1002 to S06-1006. o-Phenylenediamine (1 mmol) and benzaldehyde or furan-3-carbaldehyde or 2-nitrobenzaldehyde (1 mmol) were dissolved in 10 mL of DMF, followed by addition of sodium bisulfite (0.3 mmol). The reaction was stirred at 80 °C for 5 h, and its completion was monitored by TLC. Thereafter, the solvent was dripped into stirred water (15 mL) to precipitate a large amount of solid. The crude products **3a−5a** were obtained by filtration and used for subsequent reaction without purification.

The products **3a−5a** (1 mmol) obtained in the last step were dissolved in 50 mL of acetonitrile, followed by addition of cesium carbonate (2 mmol). The mixture was stirred for 15 min, and then ethyl carbonobromidate (2.5 mmol) was added dropwise. The reaction was stirred at room temperature for another 30 min and completed by thin-layer chromatography (TLC). The solvent was evaporated under a vacuum to give the crude solid product. Subsequently, the solid was again dissolved in 50 mL of DCM and then washed with saturated sodium bicarbonate (aq, 3 × 50 mL). The organic layer was then dried over sodium sulfate and filtered. The solvent was evaporated under a vacuum to give the crude product, which was further purified by column chromatography on silica gel (DCM/MeOH = 100:1, v/v) to obtain the desired products **3b−5b**.

3b−5b (1 mmol) were dissolved in a 12 mL mixed solvent of THF/ MeOH (3:1, v/v). Later, 12 mL of 1 N LiOH·H$_2$O (aq) was dropped into the reaction solvent at 0 °C. The reaction was stirred at room temperature overnight and evaporated under a vacuum to remove the organic layer. The solvent was adjusted to pH = 2 with 9 M hydrochloric acid and filtered to give the crude products **3c−5c**.

6-Aminoquinoline (1 mmol) was dissolved in 10 mL of DMF, followed by addition of N,N-diisopropylethylamine (DIEA, 1 mmol). The solvent was stirred at room temperature for 15 min before addition of **3c−5c** (1 mmol) and HATU (1 mmol). The reaction was then stirred overnight at room temperature. Thereafter, 25 mL of water and 25 mL of ethyl acetate were added to the solution and the water phase was washed by 25 mL of ethyl acetate. The organic layer was collected and dried over sodium sulfate. The solvent was evaporated under a vacuum to give the crude product, which was further purified by column chromatography on silica gel (DCM/MeOH = 50:1, v/v) to obtain the products **S06-1003** to **S06-1005**.

Compound **S06-1006** was obtained by reduction of **S06-1005**. Compound **S06-1005** was dissolved in 10 mL of THF, followed by addition of palladium 10% on carbon and N$_2$H$_4$·H$_2$O at 0 °C. The reaction was refluxed and completed by a TLC monitor. The reaction was filtered, and the filtrate was evaporated under a vacuum and purified by column chromatography on silica gel (DCM/MeOH = 30:1, v/v) to obtain the desired product **S06-1006**.

4.1.2.1. 2-(2-(Furan-2-yl)-1H-benzo[d]imidazol-1-yl)-N-(quinolin-6-yl) Acetamide (S06-1003). According to the general procedure described above, compound **S06-1003** was synthesized with 6-aminoquinoline and **3c**. The product **S06-1003** was further purified by column chromatography (DCM/MeOH = 50:1, v/v), with a yield of 80%, mp 238−241 °C, 95.4% HPLC purity. ^{1}H NMR (300 MHz, DMSO-d_6): δ = 10.93 (s, 1H), 8.82 (dd, J = 4.2, 1.7 Hz, 1H), 8.36 (d, J = 2.3 Hz, 1H), 8.28 (m, 1H), 8.04 (d, J = 9.1 Hz, 1H), 7.96 (d, J = 1.7 Hz, 1H), 7.86 (dd, J = 9.1, 2.4 Hz, 1H), 7.71 (qd, J = 4.1, 1.3 Hz, 2H), 7.50 (dd, J = 8.3, 4.2 Hz, 1H), 7.32 (m, 2H), 7.25 (d, J = 3.5 Hz, 1H), 6.76 (dd, J = 3.5, 1.8 Hz, 1H), 5.53 (s, 2H) ppm. ^{13}C NMR (125 MHz, DMSO-d_6): δ = 166.6, 149.7, 145.7, 145.4, 145.3, 144.7, 142.9, 137.0, 136.8, 136.0, 130.2, 128.8, 123.7, 123.3, 122.9, 122.3, 119.4, 115.7, 112.9, 112.6, 110.9, 48.1 ppm. HRMS (m/z): calcd for C$_{22}$H$_{16}$N$_4$O$_2$ [M + H]$^+$ 369.1346; found, 369.1354.

4.1.2.2. 2-(2-Phenyl-1H-benzo[d]imidazol-1-yl)-N-(quinolin-6-yl) Acetamide (S06-1004). According to the general procedure described above, compound **S06-1004** was synthesized with 6-aminoquinoline and **4c**. The product **S06-1004** was further purified by column chromatography (DCM/MeOH = 50:1, v/v), with a yield of 87%, mp 256−259.5 °C, 95.0% HPLC purity. ^{1}H NMR (300 MHz, DMSO-d_6): δ = 10.89 (s, 1H), 8.82 (dd, J = 4.2, 1.7 Hz, 1H), 8.38 (d, J = 2.3 Hz, 1H), 8.30 (m, 1H), 8.03 (d, J = 9.0 Hz, 1H), 7.84 (td, J = 6.7, 5.9, 3.7 Hz, 3H), 7.76 (m, 1H), 7.61 (m, 4H), 7.50 (dd, J = 8.3, 4.2 Hz, 1H), 7.35 (m, 2H), 5.26 (s, 2H) ppm. ^{13}C NMR (125 MHz, DMSO-d_6): δ = 166.6, 154.1, 149.8, 145.3, 143.0, 137.0, 136.8, 136.0, 130.6, 130.3, 130.2, 129.6, 129.3, 128.7, 123.7, 123.2, 122.7, 122.4, 119.6, 115.9, 111.1, 48.2 ppm. HRMS (m/z): calcd for C$_{24}$H$_{18}$N$_4$O [M + H]$^+$ 379.1551; found, 379.1559.

4.1.2.3. 2-(2-(2-Nitrophenyl)-1H-benzo[d]imidazol-1-yl)-N-(qui-nolin-6-yl) Acetamide (S06-1005). According to the general procedure described above, compound **S06-1005** was synthesized with 6-aminoquinoline and **5c**. The product **S06-1005** was further purified by column chromatography (DCM/MeOH = 45:1, v/v), with a yield of 84%, mp 246−249.5 °C, 98.8% HPLC purity. ^{1}H NMR (300 MHz, DMSO-d_6): δ = 10.72 (s, 1H), 8.80 (dd, J = 4.3, 1.7 Hz, 1H), 8.32 (d, J = 2.4 Hz, 1H), 8.28 (ddd, J = 7.8, 6.0, 1.5 Hz, 2H), 8.00 (d, J = 9.0 Hz, 1H), 7.92 (td, J = 7.5, 1.3 Hz, 1H), 7.85 (m, 2H), 7.75 (dd, J = 9.1, 2.4 Hz, 1H), 7.71 (d, J = 7.9 Hz, 1H), 7.67 (d, J = 8.0 Hz, 1H), 7.49 (dd, J = 8.3, 4.2 Hz, 1H), 7.36 (t, J = 7.5 Hz, 1H), 7.31 (t, J = 7.6 Hz, 1H), 5.13 (s, 2H) ppm. ^{13}C NMR (125 MHz, DMSO-d_6): δ = 166.2, 149.9, 149.5, 149.3, 144.4, 142.7, 137.0, 136.9, 136.0, 134.2, 132.9, 132.2, 129.5, 128.8, 125.3, 125.0, 124.1, 123.6, 122.8, 122.4, 119.7, 115.9, 111.3, 47.7 ppm. HRMS (m/z): calcd for C$_{24}$H$_{17}$N$_5$O$_3$ [M + H]$^+$ 424.1404; found, 424.1421.

4.1.2.4. 2-(2-(2-Aminophenyl)-1H-benzo[d]imidazol-1-yl)-N-(qui-nolin-6-yl) Acetamide (S06-1006). According to the general procedure described above, compound **S06-1006** was synthesized by reduction of **S06-1005**. The product **S06-1006** was further purified by column chromatography (DCM/MeOH = 30:1, v/v), with a yield of 60%, mp 240−242.5 °C, 95.9% HPLC purity. ^{1}H NMR (300 MHz, DMSO-d_6): δ = 10.91 (d, J = 6.4 Hz, 1H), 8.82 (dd, J = 4.2, 1.7 Hz, 1H), 8.38 (d, J = 2.4 Hz, 1H), 8.30 (dd, J = 8.5, 1.8 Hz, 1H), 8.03 (d, J = 9.1 Hz, 1H), 7.85 (m, 1H), 7.75 (dd, J = 6.2, 2.9 Hz, 1H), 7.61 (m, 1H), 7.50 (dd, J = 8.4, 4.2 Hz, 1H), 7.33 (m, 3H), 7.23 (m, 1H), 6.90 (d, J = 8.2 Hz, 1H), 6.70 (m, 1H), 5.84 (s, 2H), 5.17 (s, 2H) ppm. ^{13}C NMR (125 MHz, DMSO-d_6): δ = 166.7, 153.1, 149.8, 148.4, 145.3, 142.8, 136.8, 136.3, 136.0, 131.1, 130.4, 130.2, 128.8, 123.7, 122.9, 122.5, 122.3, 119.2, 116.3, 116.2, 115.9, 112.7, 111.1, 48.2 ppm. HRMS (m/z): calcd for C$_{24}$H$_{19}$N$_5$O [M + H]$^+$ 394.1662; found, 394.1675.

4.1.3. General Synthetic Procedure for Compounds S06-1002, S06-1007, and S06-1008. 6-Aminoquinoline (1 mmol) was diluted in chloroform (4 mL), and sodium bicarbonate (1.2 mmol) was added. The mixture was stirred at room temperature for 15 min before chloroacetyl chloride (1.5 mmol) was dropped in. The reaction was stirred at room temperature for 4 h and then monitored by TLC. The solution was diluted with chloroform (10 mL) and washed with water (2 × 15 mL), dried over sodium sulfate, and filtered. The solvent was evaporated under a vacuum to give the crude product **2a**, which was used for subsequent reaction without purification. **7a** and **8a** were synthesized with 3-chloropropionyl chloride and 5-chlorovaleryl chloride replacing chloroacetyl chloride.

2-Benzimidazolylacetonitrile (1 mmol) was dissolved with acetic acid (3 mL), followed by dropping sodium nitrite (1 mmol) in water under an ice bath. The mixture was stirred under an ice bath for 40 min, filtered, and washed with ice-water once and ether twice. In another reactive flask, to an ice-cooled stirred solution of hydroxylamine hydrochloride (1.2 mmol) in 1.5 mL of water, potassium hydroxide (1.5 mmol) was slowly added. Then, 1 mL of diglyme and the above residue were added. The ice bath was removed, and the reaction mixture was heated to 110 °C for 6 h. After cooling to room temperature, the reaction mixture was filtered and the residue was washed with water to give the product **1b** as a pale-yellow solid.

Compound **2a**, **7a**, or **8a** (1 mmol) was dissolved in DMF (12 mL). Cesium carbonate (1 mmol) and intermediate compound **1b** (0.9 mmol) were successively added. The solution was stirred at 70 °C for 9 h, and the completion of the reaction was monitored by TLC. Then, 80 mL of water was added into the reaction to produce a large amount of precipitation. The mixture was filtered and the residue was washed with water and methanol to produce the desired products **S06-1002**, **S06-1007**, and **S06-1008** as a yellow solid.

4.1.3.1. 2-(2-(4-Amino-1,2,5-oxadiazol-3-yl)-1H-benzo[d]-imidazol-1-yl)-N-(quinolin-6-yl)acetamide (S06-1002). According to the general procedure described above, compound **S06-1002** was synthesized with **2a** and **1b**. The product **S06-1002** was further purified by column chromatography (DCM/MeOH = 70:1, v/v) with a yield of 70%, mp 282−284 °C, 96.2% HPLC purity. ^{1}H NMR (300 MHz, DMSO-d_6): δ = 10.95 (s, 1H), 8.80 (s, 1H), 8.33 (s, 1H), 8.24 (d, J = 8.34 Hz, 1H), 8.02 (d, J = 9.39 Hz, 1H), 7.91−7.81 (m, 3H) 7.49−7.38 (m, 3H), 7.05 (s, 2H), 5.69 (s, 2H) ppm. ^{13}C NMR (125 MHz, DMSO-d_6): δ = 166.0, 156.5, 149.7, 145.2, 142.0, 141.9, 138.8, 136.9, 136.6, 136.0, 130.2, 128.8, 125.2, 123.7, 123.5, 122.3, 120.4, 115.6, 111.5, 48.7 ppm. HRMS (m/z): calcd for C$_{20}$H$_{15}$N$_7$O$_2$ [M + H]$^+$ 386.1365; found, 386.1359.

4.1.3.2. 3-(2-(4-Amino-1,2,5-oxadiazol-3-yl)-1H-benzo[d]-imidazol-1-yl)-N-(quinolin-6-yl)propenamide (S06-1007). According to the general procedure described above, compound **S06-1007** was synthesized with **7a** and **1b**, with a yield of 39%, mp 235−237 °C, 98.7% HPLC purity. ^{1}H NMR (300 MHz, DMSO-d_6): δ = 10.30 (s, 1H), 8.76 (dd, J = 1.56, 4.14 Hz, 1H), 8.25−8.21 (m, 2H), 7.91 (d, J = 9.06 Hz, 1H), 7.83 (dd, J = 8.13, 13.59 Hz, 2H), 7.65 (dd, J = 2.28, 9.06 Hz, 1H), 7.47 (q, J = 3.54 Hz, 1H), 7.40 (d, J = 7.26 Hz, 1H) 7.32 (t, J = 7.38 Hz, 1H), 7.01 (s, 2H), 5.02 (t, J = 6.66 Hz, 2H), 3.03 (t, J = 6.54 Hz, 2H). ^{13}C NMR (125 MHz, DMSO-d_6): δ = 169.4, 156.6, 149.5, 145.1, 142.1, 141.1, 138.7, 137.1, 135.9, 135.6, 129.9, 128.7, 125.0, 123.7, 123.6, 122.2, 120.3, 115.5, 112.0, 42.0, 36.9 ppm. HRMS (m/z): calcd for C$_{21}$H$_{17}$N$_7$O$_2$ [M + H]$^+$ 400.1522; found, 400.1523.

4.1.3.3. 5-(2-(4-Amino-1,2,5-oxadiazol-3-yl)-1H-benzo[d]-imidazol-1-yl)-N-(quinolin-6-yl)pentanamide (S06-1008). According to the general procedure described above, compound **S06-1008** was synthesized with **8a** and **1b**, with a yield of 45%, mp 219.5−223 °C, 98.6% HPLC purity. ^{1}H NMR (300 MHz, DMSO-d_6): δ = 10.25 (s, 1H), 8.78 (d, J = 3.60 Hz, 1H), 8.37 (s, 1H), 8.26 (d, J = 8.19 Hz, 1H), 7.95 (d, J = 8.91 Hz, 1H), 7.85 (d, J = 7.92 Hz, 2H), 7.76 (d, J = 9.12 Hz, 1H), 7.49−7.35 (m, 3H), 7.04 (s, 2H), 4.74 (t, J = 6.81 Hz, 2H), 2.44 (t, J = 7.35 Hz, 2H), 1.96−1.86 (m, 2H), 1.76−1.66 (m, 2H) ppm. ^{13}C NMR (125 MHz, DMSO-d_6): δ = 171.8, 156.6, 149.3, 145.1, 142.1, 140.9, 138.6, 137.5, 135.8, 135.7, 129.9, 128.8, 125.0, 123.7, 123.6, 122.1, 120.5, 115.2, 111.7, 45.3, 36.4, 29.5, 22.7 ppm. HRMS (m/z): calcd for C$_{23}$H$_{21}$N$_7$O$_2$ [M + H]$^+$ 428.1835; found, 428.1836.

4.1.4. General Synthetic Procedure for Compounds S06-1009 to S06-1042. The synthesis approaches of compounds S06-1009 to S06-1042 were similar to that of **S06-1002**, replacing the initial reactant 6-aminoquinoline with diverse commercially available aromatic amines. Similar to the compound **S06-1006**, **S06-1033** was obtained by reduction of **S06-1032** under the same reaction condition.

4.1.4.1. 2-(2-(4-Amino-1,2,5-oxadiazol-3-yl)-1H-benzo[d]-imidazol-1-yl)-N-(quinolin-5-yl)acetamide (S06-1009). According to the general procedure described above, compound **S06-1009** was synthesized with **9a** and **1b**. The product **S06-1009** was further purified by column chromatography (DCM/MeOH = 70:1, v/v) with a yield of 48%, mp 295−298.5 °C, 95.1% HPLC purity. ^{1}H NMR (300 MHz, DMSO-d_6): δ = 10.86 (s, 1H), 8.78 (d, J = 5.01 Hz, 1H), 8.52 (d, J = 8.25 Hz, 1H), 8.04 (d, J = 7.77 Hz, 1H), 7.97 (d, J = 5.01 Hz, 1H), 7.90 (d, J = 8.61 Hz, 2H), 7.85−7.80 (m, 1H), 7.76−7.71 (m, 1H), 7.49−7.38 (m, 2H), 7.03 (s, 2H), 5.85 (s, 2H) ppm. ^{13}C NMR (125 MHz, DMSO-d_6): δ = 166.0, 156.5, 149.7, 145.2, 142.0, 141.9, 138.8, 136.9, 136.6, 136.0, 130.2, 128.8, 125.2, 123.7, 123.5, 122.3, 120.4, 155.6, 111.7, 48.7 ppm. HRMS (m/z): calcd for C$_{20}$H$_{15}$N$_7$O$_2$ [M + H]$^+$ 386.1360; found, 386.1369.

4.1.4.2. 2-(2-(4-Amino-1,2,5-oxadiazol-3-yl)-1H-benzo[d]-imidazol-1-yl)-N-(quinolin-4-yl)acetamide (S06-1010). According to the general procedure described above, compound **S06-1010** was synthesized with **10a** and **1b**. The product **S06-1010** was further purified by column chromatography (DCM/MeOH = 50:1, v/v) with a yield of 32%, mp 289−291 °C, 95.6% HPLC purity. ^{1}H NMR (300 MHz, DMSO-d_6): δ = 10.86 (s, 1H), 8.77 (d, J = 4.98 Hz, 1H), 8.51 (d, J = 8.19 Hz, 1H), 8.04 (d, J = 8.40 Hz, 1H), 7.96 (d, J = 5.01 Hz, 1H), 7.89 (d, J = 8.49 Hz, 2H), 7.85−7.80 (m, 1H), 7.65 (t, J = 7.25 Hz, 1H, ArH), 7.47−7.40 (m, 2H), 7.01 (s, 2H), 5.85 (s, 2H) ppm. ^{13}C NMR (125 MHz, DMSO-d_6): δ = 167.3, 156.5, 155.9, 151.3, 149.1, 142.0, 141.8, 141.5, 138.8, 136.5, 130.1, 130.0, 126.6, 125.2, 123.8, 122.8, 121.2, 120.5, 111.6, 49.0 ppm. HRMS (m/z): calcd for C$_{20}$H$_{15}$N$_7$O$_2$ [M + H]$^+$ 386.1360; found, 386.1362.

4.1.4.3. 2-(2-(4-Amino-1,2,5-oxadiazol-3-yl)-1H-benzo[d]-imidazol-1-yl)-N-(quinolin-3-yl)acetamide (S06-1011). According to the general procedure described above, compound **S06-1011** was synthesized with **11a** and **1b**, with a yield of 82%, mp 293−294 °C, 96.7% HPLC purity. ^{1}H NMR (300 MHz, DMSO-d_6): δ = 11.12 (s, 1H), 8.97 (d, J = 2.43 Hz, 1H), 8.64 (d, J = 2.19 Hz, 1H), 7.93 (d, J = 8.28 Hz, 1H), 7.91−7.86 (m, 3H), 7.68−7.62 (m, 1H), 7.58−7.53 (m, 1H), 7.49−7.38 (m, 2H), 7.04 (s, 2H), 5.71 (s, 2H) ppm. ^{13}C NMR (125 MHz, DMSO-d_6): δ = 166.6, 156.5, 144.8, 144.6, 142.0, 141.8, 138.8, 136.6, 132.8, 129.0, 128.5, 128.2, 128.2, 127.6, 125.2, 123.7, 122.7, 120.4, 111.7, 48.7 ppm. HRMS (m/z): calcd for C$_{20}$H$_{15}$N$_7$O$_2$ [M + H]$^+$ 386.1360; found, 386.1365.

4.1.4.4. 2-(2-(4-Amino-1,2,5-oxadiazol-3-yl)-1H-benzo[d]-imidazol-1-yl)-N-(quinolin-2-yl)acetamide (S06-1012). According to the general procedure described above, compound **S06-1012** was synthesized with **12a** and **1b**, with a yield of 52%, mp 249−250 °C, 98.2% HPLC purity. ^{1}H NMR (300 MHz, DMSO-d_6): δ =11.46 (s, 1H), 8.33 (d, J = 9.03 Hz, 1H), 8.10 (d, J = 8.76 Hz, 1H), 7.88 (dd, J = 9.21, 16.31 Hz, 3H), 7.74 (t, J = 8.28 Hz, 1H), 7.54−7.37 (m, 3H), 7.01 (s, 2H), 6.84 (s, 1H), 5.75 (s, 2H) ppm. ^{13}C NMR (125 MHz, DMSO-d_6): δ = 167.2, 156.5, 151.6, 146.8, 142.0, 141.9, 139.1, 138.8, 136.5, 130.6, 128.3, 127.5, 126.1, 125.6, 125.2, 123.7, 120.4, 114.5, 111.6, 48.8 ppm. HRMS (m/z): calcd for C$_{20}$H$_{15}$N$_7$O$_2$ [M + H]$^+$ 386.1360; found, 386.1361.

4.1.4.5. 2-(2-(4-Amino-1,2,5-oxadiazol-3-yl)-1H-benzo[d]-imidazol-1-yl)-N-(naphthalen-2-yl)acetamide (S06-1013). According to the general procedure described above, compound **S06-1013** was synthesized with **13a** and **1b**, with a yield of 78%, mp 300−303 °C, 97.0% HPLC purity. ^{1}H NMR (300 MHz, DMSO-d_6): δ = 10.81 (s, 1H), 8.25 (d, J = 1.65 Hz, 1H), 7.91−7.83 (m, 4H), 7.77 (d, J = 7.83 Hz, 1H), 7.61 (dd, J = 2.07, 8.85 Hz, 1H), 7.48−7.38 (m, 4H), 7.05 (s, 2H), 5.67 (s, 2H) ppm. ^{13}C NMR (125 MHz, DMSO-d_6): δ = 165.8, 156.5, 142.0, 141.9, 138.8, 136.7, 136.6, 133.8, 130.3, 129.0, 127.9, 127.8, 127.0, 125.2, 125.2, 123.7, 120.4, 120.2, 115.8, 111.7, 48.7 ppm. HRMS (m/z): calcd for C$_{21}$H$_{16}$N$_6$O$_2$ [M + H]$^+$ 385.1408; found, 385.1411.

4.1.4.6. 2-(2-(4-Amino-1,2,5-oxadiazol-3-yl)-1H-benzo[d]-imidazol-1-yl)-N-(naphthalen-1-yl)acetamide (S06-1014). According to the general procedure described above, compound **S06-1014** was synthesized with **14a** and **1b**, with a yield of 72%, mp 273−274 °C, 95.3% HPLC purity. ¹H NMR (300 MHz, DMSO-d_6): δ = 10.47 (s, 1H), 8.23 (d, J = 7.59 Hz, 1H), 7.97−7.87 (m, 3H), 7.79 (d, J = 7.92 Hz, 1H), 7.54−7.65 (m, 3H), 7.48 (t, J = 7.68 Hz, 2H), 7.40 (t, J = 7.92 Hz, 2H) 6.99 (s, 2H), 5.78 (s, 2H) ppm. ¹³C NMR (125 MHz, DMSO-d_6): δ = 166.6, 156.6, 142.1, 142.0, 138.9, 136.6, 134.2, 133.5, 128.6, 128.4, 126.7, 126.4, 126.2, 126.0, 125.2, 123.7, 123.3, 122.3, 120.5, 111.6, 48.6 ppm. HRMS (m/z): calcd for $C_{21}H_{16}N_6O_2$ [M + H]⁺ 385.1413; found, 385.1411.

4.1.4.7. 2-(2-(4-Amino-1,2,5-oxadiazol-3-yl)-1H-benzo[d]-imidazol-1-yl)-N-(4-bromonaphthalen-1-yl)acetamide (S06-1015). According to the general procedure described above, compound **S06-1015** was synthesized with **15a** and **1b**, with a yield of 72%, mp 293−296 °C, 98.0% HPLC purity. ¹H NMR (300 MHz, DMSO-d_6): δ = 10.65 (s, 1H), 8.35−8.31 (m, 1H), 8.19−8.16 (m, 1H), 7.92 (d, J = 8.16 Hz, 1H), 7.87 (dd, J = 3.09, 8.08 Hz, 2H), 7.76−7.72 (m, 2H), 7.58 (d, J = 8.10 Hz, 1H), 7.50−7.39 (m, 2H), 7.04 (s, 2H), 5.79 (s, 2H) ppm. ¹³C NMR (125 MHz, DMSO-d_6): δ = 166.8, 156.5, 141.9, 141.8, 138.8, 136.5, 133.7, 132.0, 130.1, 129.6, 128.6, 127.5, 127.2, 125.3, 124.0, 123.8, 123.1, 120.4, 119.1, 111.5, 48.5 ppm. HRMS (m/z): calcd for $C_{21}H_{15}BrN_6O_2$ [M + H]⁺ 463.0513; found, 463.0513.

4.1.4.8. 2-(2-(4-Amino-1,2,5-oxadiazol-3-yl)-1H-benzo[d]-imidazol-1-yl)-N-phenylacetamide (S06-1016). According to the general procedure described above, compound **S06-1016** was synthesized with **16a** and **1b**, with a yield of 68%, mp 286.5−288 °C, 96.5% HPLC purity. ¹H NMR (300 MHz, DMSO-d_6): δ = 10.51 (s, 1H), 7.88 (d, J = 7.83 Hz, 1H), 7.81 (d, J = 7.89 Hz, 1H), 7.57 (d, J = 14.10 Hz, 2H), 7.47−7.39 (m, 2H), 7.36−7.29 (m, 2H), 7.07 (t, J = 7.29 Hz, 1H), 6.98 (s, 2H), 5.59 (s, 2H) ppm. ¹³C NMR (125 MHz, DMSO-d_6): δ = 165.5, 156.5, 142.0, 141.8, 139.1, 138.7, 136.6, 129.3 (2C), 125.2, 124.0, 123.7, 120.4, 119.5 (2C), 111.6, 48.6 ppm. HRMS (m/z): calcd for $C_{17}H_{14}N_6O_2$ [M + H]⁺ 335.1521; found, 334.1245.

4.1.4.9. 2-(2-(4-Amino-1,2,5-oxadiazol-3-yl)-1H-benzo[d]-imidazol-1-yl)-N-(2-fluorophenyl)acetamide (S06-1017). According to the general procedure described above, compound **S06-1017** was synthesized with **17a** and **1b**, with a yield of 73%, mp 289−291.5 °C, 97.2% HPLC purity. ¹H NMR (300 MHz, DMSO-d_6): δ = 10.42 (s, 1H), 7.87 (dd, J = 7.92, 12.66 Hz, 3H), 7.38−7.49 (m, 2H), 7.32 (t, J = 7.68 Hz, 1H), 7.17 (s, 2H), 7.03 (s, 2H), 5.69 (s, 2H) ppm. ¹³C NMR (125 MHz, DMSO-d_6): δ = 166.2, 156.5, 142.0, 141.8, 138.7, 136.5, 126.2−126.1, 125.9−125.9, 125.2, 124.9, 124.1, 123.7, 120.4, 116.1, 116.0, 111.6, 48.5 ppm. HRMS (m/z): calcd for $C_{17}H_{13}FN_6O_2$ [M + H]⁺ 353.1157; found, 353.1164.

4.1.4.10. 2-(2-(4-Amino-1,2,5-oxadiazol-3-yl)-1H-benzo[d]-imidazol-1-yl)-N-(3-fluorophenyl)acetamide (S06-1018). According to the general procedure described above, compound **S06-1018** was synthesized with **18a** and **1b**, with a yield of 62%, mp 259.5−262 °C, 96.8% HPLC purity. ¹H NMR (300 MHz, DMSO-d_6): δ = 10.99 (s, 1H), 7.86 (dd, J = 7.29, 12.51 Hz, 2H), 7.54 (d, J = 11.40 Hz, 1H), 7.34−7.47 (m, 4H), 7.02 (s, 2H), 6.87−6.94 (m, 1H), 5. 62 (s, 2H) ppm. ¹³C NMR (125 MHz, DMSO-d_6): δ = 165.9, 163.6, 161.7, 156.5, 142.0−141.9, 140.9−140.8, 138.7, 136.5, 131.0-130.9, 125.1, 123.7, 120.4, 115.4−115.4, 111.5, 110.5−110.4, 106.6−106.4, 48.7 ppm. HRMS (m/z): calcd for $C_{17}H_{13}FN_6O_2$ [M + H]⁺ 353.1157; found, 353.1166.

4.1.4.11. 2-(2-(4-Amino-1,2,5-oxadiazol-3-yl)-1H-benzo[d]-imidazol-1-yl)-N-(2,3-difluorophenyl)acetamide (S06-1019). According to the general procedure described above, compound **S06-1019** was synthesized with **19a** and **1b**, with a yield of 78%, mp 283−286.5 °C, 95.3% HPLC purity. ¹H NMR (300 MHz, DMSO-d_6): δ =10.66 (s, 1H), 7.90 (t, J = 8.34 Hz, 2H), 7.69 (t, J = 7.65 Hz, 1H), 7.52−7.40 (m, 2H), 7.25−7.17 (m, 2H), 7.05 (s, 2H), 5.73 (s, 2H) ppm. ¹³C NMR (125 MHz, DMSO-d_6): δ = 166.4, 156.5, 151.5−151.4, 149.6−149.5, 142.0, 141.8, 138.7, 136.5, 128.2-128.1, 125.2, 124.8−124.7, 123.7, 120.4, 119.4, 113.2−113.0, 111.5, 48.6 ppm. HRMS (m/z): calcd for $C_{17}H_{12}F_2N_6O_2$ [M + H]⁺ 371.1096; found, 371.1067.

4.1.4.12. 2-(2-(4-Amino-1,2,5-oxadiazol-3-yl)-1H-benzo[d]-imidazol-1-yl)-N-(2-chlorophenyl)acetamide (S06-1020). According to the general procedure described above, compound **S06-1020** was synthesized with **20a** and **1b**, with a yield of 66%, mp 284−288 °C, 95.1% HPLC purity. ¹H NMR (300 MHz, DMSO-d_6): δ = 10.09 (s, 1H), 7.84 (q, J = 7.53 Hz, 2H), 7.67 (dd, J = 1.59, 8.03 Hz, 1H), 7.53−7.36 (m, 3H), 7.34−7.28 (m, 1H), 7.23−7.17 (m, 1H), 6.96 (s, 2H), 5.68 (s, H) ppm. ¹³C NMR (125 MHz, DMSO-d_6): δ = 166.2, 156.5, 155.9, 142.0, 141.9, 140.7, 139.0, 138.7, 136.4, 134.9, 130.1, 127.9, 125.2, 123.7, 120.4, 111.5, 48.5 ppm. HRMS (m/z): calcd for $C_{17}H_{13}ClN_6O_2$ [M + H]⁺ 369.0867; found, 369.0862.

4.1.4.13. 2-(2-(4-Amino-1,2,5-oxadiazol-3-yl)-1H-benzo[d]-imidazol-1-yl)-N-(3-chlorophenyl)acetamide (S06-1021). According to the general procedure described above, compound **S06-1021** was synthesized with **21a** and **1b**, with a yield of 72%, mp 283−285 °C, 98.9% HPLC purity. ¹H NMR (300 MHz, DMSO-d_6): δ = 10.80 (s, 1H), 7.88 (q, J = 7.89 Hz, 2H), 7.79 (s, 1H), 7.49−7.39 (m, 4H), 7.17 (d, J = 7.80 Hz, 1H), 7. 05 (s, 2H), 5.63 (s, 2H) ppm. ¹³C NMR (125 MHz, DMSO-d_6): δ = 166.0, 156.5, 141.9, 141.8, 140.5, 138.7, 136.5, 133.7, 131.1, 125.2, 123.8, 123.7, 120.4, 119.0, 118.0, 111.6, 48.6 ppm. HRMS (m/z): calcd for $C_{17}H_{13}ClN_6O_2$ [M + H]⁺ 369.0861; found, 369.0863.

4.1.4.14. 2-(2-(4-Amino-1,2,5-oxadiazol-3-yl)-1H-benzo[d]-imidazol-1-yl)-N-(4-chlorophenyl)acetamide (S06-1022). According to the general procedure described above, compound **S06-1022** was synthesized with **22a** and **1b**, with a yield of 54%, mp 288.5−290 °C, 98.2% HPLC purity. ¹H NMR (300 MHz, DMSO-d_6): δ = 10.71 (s, 1H), 7.86 (q, J = 8.13 Hz, 2H), 7.53 (dd, J = 8.85, 15.09 Hz, 4H), 7.47−7.36 (m, 2H), 7.02 (s, 2H), 5. 59 (s, 2H) ppm. ¹³C NMR (125 MHz, DMSO-d_6): δ = 165.7, 156.5, 141.9, 141.8, 138.7, 138.5, 136.5, 132.2 (2C), 125.2, 123.7, 121.5 (2C), 120.4, 115.6, 111.6, 48.7 ppm. HRMS (m/z): calcd for $C_{17}H_{13}ClN_6O_2$ [M + H]⁺ 369.0867; found, 369.0866.

4.1.4.15. 2-(2-(4-Amino-1,2,5-oxadiazol-3-yl)-1H-benzo[d]-imidazol-1-yl)-N-(3-bromophenyl)acetamide (S06-1023). According to the general procedure described above, compound **S06-1023** was synthesized with **23a** and **1b**, with a yield of 58%, mp 278−281 °C, 96.1% HPLC purity. ¹H NMR (300 MHz, DMSO-d_6): δ = 10.81 (s, 1H), 7.94−7.84 (m, 3H), 7.53−7.41 (m, 3H), 7.32 (d, J = 7.47 Hz, 2H), 7.06 (s, 2H), 5.63 (s, 2H) ppm. ¹³C NMR (125 MHz, DMSO-d_6): δ = 166.0, 156.5, 141.9, 141.8, 140.6, 138.7, 136.5, 131.4, 126.7, 125.2, 123.7, 122.1, 121.9, 120.4, 118.3, 111.6, 48.6 ppm. HRMS (m/z): calcd for $C_{17}H_{13}BrN_6O_2$ [M + H]⁺ 415.0356; found, 415.1521.

4.1.4.16. 2-(2-(4-Amino-1,2,5-oxadiazol-3-yl)-1H-benzo[d]-imidazol-1-yl)-N-(4-bromophenyl)acetamide (S06-1024). According to the general procedure described above, compound **S06-1024** was synthesized with **24a** and **1b**, with a yield of 45%, mp 279.5−284 °C, 98.6% HPLC purity. ¹H NMR (300 MHz, DMSO-d_6): δ = 10.70 (s, 1H), 7.85 (q, J = 7.59 Hz, 2H), 7.60 (d, J = 8.85 Hz, 2H), 7.45−7.36 (m, 4H), 7.01 (s, 2H), 5.59 (s, 2H) ppm. ¹³C NMR (125 MHz, DMSO-d_6): δ = 165.7, 156.5, 142.0, 141.8, 138.7, 138.0, 136.5, 129.3 (2C), 127.6, 125.2, 123.7, 121.1 (2C), 120.4, 111.6, 48.6 ppm. HRMS (m/z): calcd for $C_{17}H_{13}BrN_6O_2$ [M + H]⁺ 413.0356; found, 413.0356.

4.1.4.17. 2-(2-(4-Amino-1,2,5-oxadiazol-3-yl)-1H-benzo[d]-imidazol-1-yl)-N-(m-tolyl)acetamide (S06-1025). According to the general procedure described above, compound **S06-1025** was synthesized with **25a** and **1b**, with a yield of 55%, mp 282−286.5 °C, 97.0% HPLC purity. ¹H NMR (300 MHz, DMSO-d_6): δ = 10.49 (s, 1H), 7.85 (q, J = 7.23 Hz, 2H), 7.47−7.33 (m, 4H), 7.19 (t, J = 7.68 Hz, 1H), 7.02 (s, 2H), 6.89 (d, J = 7.53 Hz, 1H), 5.58 (s, 2H), 2.26 (s, 3H) ppm. ¹³C NMR (125 MHz, DMSO-d_6): δ = 165.4, 156.5, 142.0, 141.9, 139.0, 138.7, 138.6, 136.6, 128.1, 125.1, 124.7, 123.7, 120.4, 120.1, 116.7, 111.6, 48.6, 21.6 ppm. HRMS (m/z): calcd for $C_{18}H_{16}N_6O_2$ [M + H]⁺ 349.1408; found, 349.1413.

4.1.4.18. 2-(2-(4-Amino-1,2,5-oxadiazol-3-yl)-1H-benzo[d]-imidazol-1-yl)-N-(p-tolyl)acetamide (S06-1026). According to the general procedure described above, compound **S06-1026** was synthesized with **26a** and **1b**, with a yield of 62%, mp 276−277 °C, 96.3% HPLC purity. ¹H NMR (300 MHz, DMSO-d_6): δ = 10.46 (s, 1H), 7.85 (q, J = 7.44 Hz, 2H), 7.47−7.36 (m, 4H), 7.12 (d, J = 8.34 Hz, 2H), 7.02 (s, 2H), 5. 57 (s, 2H), 2.25 (s, 3H) ppm. ¹³C NMR (125

MHz, DMSO-d_6): δ = 165.2, 156.5, 142.0, 141.8, 138.7, 136.6, 136.6, 133.0, 127.0 (2C), 125.1, 123.6, 120.4, 119.5 (2C), 111.6, 48.6, 20.9 ppm. HRMS (m/z): calcd for $C_{18}H_{16}N_6O_2$ [M + H]$^+$ 349.1408; found, 349.1408.

4.1.4.19. 2-(2-(4-Amino-1,2,5-oxadiazol-3-yl)-1H-benzo[d]-imidazol-1-yl)-N-(2,3-dimethylphenyl)acetamide (S06-1027). According to the general procedure described above, compound S06-1027 was synthesized with 27a and 1b, with a yield of 60%, mp 289−290.5 °C, 98.7% HPLC purity. ^{1}H NMR (300 MHz, DMSO-d_6): δ = 9.94 (s, 1H), 7.86 (q, J = 4.74 Hz, 2H), 7.48 (t, J = 6.90 Hz, 1H), 7.36 (t, J = 6.87 Hz, 1H), 7.08 (t, J = 3.18 Hz, 1H), 7.01−7.04 (m, 4H), 5.62 (s, 2H), 2.24 (s, 3H), 2.13 (s, 3H) ppm. ^{13}C NMR (125 MHz, DMSO-d_6): δ = 165.8, 156.5, 142.0, 141.9, 138.7, 137.6, 136.6, 135.9, 131.8, 127.6, 125.7, 125.1, 124.0, 123.6, 120.4, 111.6, 48.3, 20.6, 14.4 ppm. HRMS (m/z): calcd for $C_{19}H_{18}N_6O_2$ [M + H]$^+$ 363.1564; found, 363.1574.

4.1.4.20. 2-(2-(4-Amino-1,2,5-oxadiazol-3-yl)-1H-benzo[d]-imidazol-1-yl)-N-(3-methoxyphenyl)acetamide (S06-1028). According to the general procedure described above, compound S06-1028 was synthesized with 28a and 1b, with a yield of 52%, mp 284−288 °C, 98.7% HPLC purity. ^{1}H NMR (300 MHz, DMSO-d_6): δ = 10.57 (s, 1H), 7.85 (q, J = 7.41 Hz, 2H), 7.48−7.36 (m, 2H), 7.29 (t, J = 2.13 Hz, 1H), 7.23 (t, J = 8.13 Hz, 1H), 7.11 (d, J = 8.07 Hz, 1H), 7.03 (s, 2H), 6.65 (dd, J = 2.34, 7.92 Hz, 1H), 5. 59 (s, 2H), 3.70 (s, 3H) ppm. ^{13}C NMR (125 MHz, DMSO-d_6): δ = 165.6, 160.1, 156.5, 142.0, 141.8, 140.3, 138.7, 136.6, 130.2, 125.2, 123.7, 120.4, 111.8, 111.6, 109.6, 105.2, 55.4, 48.7 ppm. HRMS (m/z): calcd for $C_{18}H_{16}N_6O_3$ [M + H]$^+$ 365.1357; found, 365.1361.

4.1.4.21. 2-(2-(4-Amino-1,2,5-oxadiazol-3-yl)-1H-benzo[d]-imidazol-1-yl)-N-(4-methoxyphenyl)acetamide (S06-1029). According to the general procedure described above, compound S06-1029 was synthesized with 29a and 1b, with a yield of 52%, mp 281−285.5 °C, 98.4% HPLC purity. ^{1}H NMR (300 MHz, DMSO-d_6): δ = 10.41 (s, 1H), 7.84 (q, J = 7.26 Hz, 2H), 7.48 (d, J = 9.09 Hz, 2H), 7.45−7.38 (m, 2H), 7.03 (s, 2H), 6.89 (d, J = 9.09 Hz, 2H), 5.56 (s, 2H), 3.72 (s, 3H) ppm. ^{13}C NMR (125 MHz, DMSO-d_6): δ = 164.9, 156.5, 155.8, 142.0, 141.9, 138.7, 136.6, 132.2, 125.1, 123.6, 121.1 (2C), 120.4, 114.4 (2C), 111.6, 55.6, 48.5 ppm. HRMS (m/z): calcd for $C_{18}H_{16}N_6O_3$ [M + H]$^+$ 365.1362; found, 365.1357.

4.1.4.22. 2-(2-(4-Amino-1,2,5-oxadiazol-3-yl)-1H-benzo[d]-imidazol-1-yl)-N-(3,4,5-trimethoxyphenyl)acetamide (S06-1030). According to the general procedure described above, compound S06-1030 was synthesized with S06-1030 and 1b, with a yield of 56%, mp 255−258 °C, 97.9% HPLC purity. ^{1}H NMR (300 MHz, DMSO-d_6): δ = 10.43 (s, 1H), 7.87 (d, J = 7.62 Hz, 1H), 7.79 (d, J = 7.47 Hz, 1H), 7.48−7.36 (m, 2H), 6.96 (s, 4H), 5. 57 (s, 2H), 3.72 (s, 6H), 3.63 (s, 3H) ppm. ^{13}C NMR (125 MHz, DMSO-d_6): δ = 165.3, 156.5, 153.3 (2C), 142.0, 141.8, 138.7, 136.5, 135.3, 134.0, 125.2, 123.7, 120.4, 111.6, 97.0 (2C), 60.6, 56.09 (2C), 48.6 ppm. HRMS (m/z): calcd for $C_{20}H_{20}N_6O_5$ [M + H]$^+$ 425.1573; found, 425.1558.

4.1.4.23. 2-(2-(4-Amino-1,2,5-oxadiazol-3-yl)-1H-benzo[d]-imidazol-1-yl)-N-(3-nitrophenyl)acetamide (S06-1031). According to the general procedure described above, compound S06-1031 was synthesized with 31a and 1b, with a yield of 64%, mp 249−253 °C, 98.1% HPLC purity. ^{1}H NMR (300 MHz, DMSO-d_6): δ = 11.12. (s, 1H), 8.61 (s, 1H), 7.98−7.86 (m, 4H), 7.68 (t, J = 7.89 Hz, 1H), 7.51−7.40 (m, 2H), 7.06 (s, 2H), 5.67 (s, 2H) ppm. ^{13}C NMR (125 MHz, DMSO-d_6): δ = 166.5, 156.5, 148.5, 141.9, 141.8, 140.1, 138.7, 136.5, 130.9, 125.5, 125.2, 123.7, 120.4, 118.6, 113.7, 111.6, 48.7 ppm. HRMS (m/z): calcd for $C_{17}H_{13}N_7O_4$ [M + H]$^+$ 380.1102; found, 380.1106.

4.1.4.24. 2-(2-(4-Amino-1,2,5-oxadiazol-3-yl)-1H-benzo[d]-imidazol-1-yl)-N-(4-nitrophenyl)acetamide (S06-1032). According to the general procedure described above, compound S06-1032 was synthesized with 32a and 1b, with a yield of 64%, mp 249−253 °C, 97.6% HPLC purity. ^{1}H NMR (300 MHz, DMSO-d_6): δ = 11.20 (s, 1H), 8.24 (d, J = 9.27 Hz, 2H), 7.90−7.80 (m, 4H), 7.48−7.37 (m, 2H), 7.01 (s, 2H), 5. 66 (s, 2H). ^{13}C NMR (125 MHz, DMSO-d_6): δ = 166.7, 156.5, 145.1, 142.9, 141.9, 141.7, 138.7, 136.5, 125.6 (2C), 125.2, 123.7, 120.4, 119.4 (2C), 111.6, 48.9 ppm. HRMS (m/z): calcd for $C_{17}H_{13}N_7O_4$ [M + H]$^+$ 380.1107; found, 380.1104.

4.1.4.25. 2-(2-(4-Amino-1,2,5-oxadiazol-3-yl)-1H-benzo[d]-imidazol-1-yl)-N-(4-aminophenyl)acetamide (S06-1033). According to the general procedure described above, compound S06-1033 was synthesized by reduction of S06-1032, with a yield of 24%, mp 231−239 °C, 95.2% HPLC purity. ^{1}H NMR (300 MHz, DMSO-d_6): δ = 10.08 (s, 1H), 7.85 (d, J = 7.05 Hz, 1H), 7.76 (d, J = 7.77 Hz, 1H), 7.40 (t, J = 8.82 Hz, 3H), 7.18 (d, J = 5.79 Hz, 2H), 6.94 (s, 2H), 6.50 (d, J = 5.82 Hz, 1H), 5.51 (s, 2H), 4.81 (s, 2H) ppm. ^{13}C NMR (125 MHz, DMSO-d_6): δ = 164.3, 156.5, 145.5, 142.0, 141.9, 138.7, 136.6, 128.2, 125.1, 123.6, 121.3 (2C), 120.4, 114.3 (2C), 111.6, 48.4 ppm. HRMS (m/z): calcd for $C_{17}H_{15}N_7O_2$ [M + H]$^+$ 350.1360; found, 350.1349.

4.1.4.26. 2-(2-(4-Amino-1,2,5-oxadiazol-3-yl)-1H-benzo[d]-imidazol-1-yl)-N-(3-cyanophenyl)acetamide (S06-1034). According to the general procedure described above, compound S06-1034 was synthesized with 34a and 1b, with a yield of 56%, mp 255−258 °C, 95.9% HPLC purity. ^{1}H NMR (300 MHz, DMSO-d_6): δ = 11.20 (s, 1H), 8.08 (s, 1H), 7.92−7.83 (m, 3H), 7.61−7.54 (m, 2H), 7.50−7.38 (m, 2H), 7.08 (s, 2H), 5.66 (s, 2H) ppm. ^{13}C NMR (125 MHz, DMSO-d_6): δ = 166.3, 156.5, 142.0, 141.8, 139.9, 138.7, 136.5, 130.8, 127.6, 125.2, 124.1, 123.7, 122.2, 120.4, 119.0, 112.2, 111.5, 48.7 ppm. HRMS (m/z): calcd for $C_{18}H_{13}N_7O_4$ [M + H]$^+$ 360.1203; found, 360.1209.

4.1.4.27. N-(3-Acetylphenyl)-2-(2-(4-amino-1,2,5-oxadiazol-3-yl)-1H-benzo[d]imidazol-1-yl)acetamide (S06-1035). According to the general procedure described above, compound S06-1035 was synthesized with 35a and 1b, with a yield of 58%, mp 285−286.5 °C, 97.1% HPLC purity. ^{1}H NMR (300 MHz, DMSO-d_6): δ = 10.85 (s, 1H), 8.21 (s, 1H), 7.87 (dd, J = 8.58, 20.55 Hz, 3H), 7.77 (d, J = 7.62 Hz, 1H), 7.53−7.41 (m, 3H), 7.07 (s, 2H), 5.64 (s, 2H), 2.56 (s, 3H) ppm. ^{13}C NMR (125 MHz, DMSO-d_6): δ = 198.0, 165.9, 156.5, 142.0, 141.8, 139.5, 138.7, 137.9, 136.6, 129.8, 125.2, 124.1, 124.0, 123.7, 120.4, 118.7, 111.6, 48.7, 27.2 ppm. HRMS (m/z): calcd for $C_{19}H_{16}N_6O_3$ [M + H]$^+$ 377.1357; found, 377.1362.

4.1.4.28. N-(4-Acetylphenyl)-2-(2-(4-amino-1,2,5-oxadiazol-3-yl)-1H-benzo[d]imidazol-1-yl)acetamide (S06-1036). According to the general procedure described above, compound S06-1036 was synthesized with 36a and 1b, with a yield of 52%, mp 292−297 °C, 97.4% HPLC purity. ^{1}H NMR (300 MHz, DMSO-d_6): δ = 10.87 (s, 1H), 7.94 (d, J = 8.67 Hz, 2H), 7.86 (dd, J = 7.44, 14.80 Hz, 2H), 7.71 (d, J = 8.79 Hz, 2H), 7.48−7.36 (m, 2H), 6.98 (s, 2H), 5.63 (s, 2H), 2.53 (s, 3H) ppm. ^{13}C NMR (125 MHz, DMSO-d_6): δ = 197.0, 166.2, 156.5, 143.4, 141.9, 141.8, 138.7, 136.5, 132.5, 130.1 (2C), 125.2, 123.7, 120.4, 118.9 (2C), 111.6, 48.8, 26.9 ppm. HRMS (m/z): calcd for $C_{19}H_{16}N_6O_3$ [M + H]$^+$ 377.1362; found, 377.1356.

4.1.4.29. Methyl 3-(2-(2-(4-Amino-1,2,5-oxadiazol-3-yl)-1H-benzo[d]imidazol-1-yl)acetamido)benzoate (S06-1037). According to the general procedure described above, compound S06-1037 was synthesized with 37a and 1b, with a yield of 52%, mp 286.5−289 °C, 95.3% HPLC purity. ^{1}H NMR (300 MHz, DMSO-d_6): δ = 10.84 (s, 1H), 8.29 (s, 1H), 7.90−7.79 (m, 3H), 7.67 (d, J = 7.83 Hz, 1H), 7.51−7.37 (m, 3H), 7.04 (s, 2H), 5.62 (s, 2H), 3.83 (s, 3H) ppm. ^{13}C NMR (125 MHz, DMSO-d_6): δ = 166.5, 165.9, 156.4, 141.9, 141.8, 139.3, 138.7, 136.4, 130.7, 129.9, 125.3, 124.7, 124.1, 123.8, 120.4, 120.0, 111.4, 52.7, 48.5 ppm. HRMS (m/z): calcd for $C_{19}H_{16}N_6O_4$ [M + H]$^+$ 393.1306; found, 393.1314.

4.1.4.30. Methyl 4-(2-(2-(4-Amino-1,2,5-oxadiazol-3-yl)-1H-benzo[d]imidazol-1-yl)acetamido)benzoate (S06-1038). According to the general procedure described above, compound S06-1038 was synthesized with 38a and 1b, with a yield of 58%, mp 285.5−288 °C, 96.7% HPLC purity. ^{1}H NMR (300 MHz, DMSO-d_6): δ = 10.99 (s, 1H), 7.96 (d, J = 8.70 Hz, 2H), 7.89 (t, J = 8.88 Hz, 2H), 7.74 (d, J = 8.64 Hz, 2H), 7.50−7.39 (m, 2H), 7.06 (s, 2H), 5. 65 (s, 2H), 3.84 (s, 3H) ppm. ^{13}C NMR (125 MHz, DMSO-d_6): δ = 166.2 (2C), 156.5, 143.4, 141.9, 141.8, 138.7, 136.5, 130.9 (2C), 125.2, 124.8, 123.7, 120.4, 119.0 (2C), 111.6, 52.4, 48.7 ppm. HRMS (m/z): calcd for $C_{19}H_{16}N_6O_4$ [M + H]$^+$ 393.1311; found, 393.1307.

4.1.4.31. N-(3-Acetamidophenyl)-2-(2-(4-amino-1,2,5-oxadiazol-3-yl)-1H-benzo[d]imidazol-1-yl)acetamide (S06-1039). According to the general procedure described above, compound S06-1039 was synthesized with 39a and 1b, with a yield of 48%, mp 292.5−295.5 °C,

97.5% HPLC purity. ^{1}H NMR (300 MHz, DMSO-d_6): δ = 10.61 (s, 1H), 9.97 (s, 1H), 7.95 (s, 1H), 7.88 (dd, J = 7.50, 12.81 Hz, 2H), 7.50−7.38 (m, 2H), 7.33−7.19 (m, 3H), 7.05 (s, 2H), 5.61 (s, 2H), 2.05 (s, 3H) ppm. ^{13}C NMR (125 MHz, DMSO-d_6): δ = 168.8, 165.5, 156.5, 141.9, 141.8, 140.1, 139.3, 138.7, 136.6, 129.4, 125.1, 123.6, 120.4, 114.6, 114.3, 111.6, 110.3, 48.6, 24.5 ppm. HRMS (m/z): calcd for $C_{19}H_{17}N_7O_3$ [M + H]$^+$ 392.1466; found, 392.1476.

4.1.4.32. N-(4-Acetamidophenyl)-2-(2-(4-amino-1,2,5-oxadiazol-3-yl)-1H-benzo[d]imidazol-1-yl)acetamide (S06-1040). According to the general procedure described above, compound **S06-1040** was synthesized with **40a** and **1b**, with a yield of 42%, mp 296.5−299 °C, 96.4% HPLC purity. ^{1}H NMR (300 MHz, DMSO-d_6): δ = 10.48 (s, 1H), 9.89 (s, 1H), 7.84 (dd, J = 5.16, 15.22 Hz, 2H), 7.49−7.39 (m, 6H), 7.02 (s, 2H), 5. 57 (s, 2H), 2.02 (s, 3H) ppm. ^{13}C NMR (125 MHz, DMSO-d_6): δ = 168.5, 165.1, 156.5, 142.0, 141.8, 138.7, 136.6, 135.6, 134.3, 125.1, 123.6, 120.4, 120.0 (2C), 119.9 (2C), 111.6, 48.5, 24.4 ppm. HRMS (m/z): calcd for $C_{19}H_{17}N_7O_3$ [M + H]$^+$ 392.1466; found, 392.1453.

4.1.4.33. N-([1,1′-Biphenyl]-4-yl)-2-(2-(4-amino-1,2,5-oxadiazol-3-yl)-1H-benzo[d]imidazol-1-yl)acetamide (S06-1041). According to the general procedure described above, compound **S06-1041** was synthesized with **41a** and **1b**, with a yield of 65%, mp 299.5−303 °C, 96.1% HPLC purity. ^{1}H NMR (300 MHz, DMSO-d_6): δ = 10.70 (s, 1H), 7.87 (t, J = 8.64 Hz, 2H), 7.70−7.63 (m, 6H), 7.49−7.33 (m, 5H), 7.04 (s, 2H), 5.62 (s, 2H) ppm. ^{13}C NMR (125 MHz, DMSO-d_6): δ = 165.6, 156.5, 142.0, 141.9, 140.0, 138.7, 138.6, 136.6, 135.7, 129.4 (2C), 127.5 (2C), 126.7 (2C), 125.2, 123.7, 120.4, 119.9 (2C), 111.6, 48.7 ppm. HRMS (m/z): calcd for $C_{23}H_{18}N_6O_2$ [M + H]$^+$ 411.1564; found, 411.1564.

4.1.4.34. 2-(2-(4-Amino-1,2,5-oxadiazol-3-yl)-1H-benzo[d]imidazol-1-yl)-N-(benzo[d][1,3]dioxol-5-yl)acetamide (S06-1042). According to the general procedure described above, compound **S06-1042** was synthesized with **42a** and **1b**, with a yield of 56%, mp 280−286 °C, 97.7% HPLC purity. ^{1}H NMR (300 MHz, DMSO-d_6): δ = 10.49 (s, 1H), 7.84 (dd, J = 7.62, 15.69 Hz, 2H), 7.47−7.36 (m, 2H), 7.24 (d, J = 1.95 Hz, 1H), 7.02 (s, 2H), 6.97 (dd, J = 2.07, 8.40 Hz, 1H), 6.87 (d, J = 8.40 Hz, 1H), 5.98 (s, 2H) 5. 55 (s, 2H). ^{13}C NMR (125 MHz, DMSO-d_6): δ = 165.1, 156.5, 147.6, 143.6, 142.0, 141.8, 138.7, 136.5, 133.5, 125.1, 123.6, 120.4, 112.4, 111.6, 108.6, 101.7, 101.5, 48.5 ppm. HRMS (m/z): calcd for $C_{18}H_{14}N_6O_4$ [M + H]$^+$ 379.1149; found, 379.1158.

4.1.5. General Synthetic Procedure for Compounds S06-1043 to S06-1046. The synthesis approaches of compounds **S06-1043** to **S06-1046** were similar to that of **S06-1002**. However, as compounds **43a** and **44a** could not be purchased, they were synthesized from 4,5-dimethyl-1,2-phenylenediamine. 4,5-Dimethyl-1,2-phenylenediamine (1 mmoL) was mixed with ethyl cyanoacetate (1.5 mmoL) and reacted under argon at 185 °C for 2 h. Completion of the reaction was monitored by TLC. Afterward, 5 mL of water was added into the reaction system and washed by ether (3 × 30 mL). The ether phase was collected, dried over sodium sulfate, and evaporated under a vacuum to give a crude product. It was subsequently purified by column chromatography on silica gel (DCM/methanol (MeOH) = 20:1, v/v) to obtain **43a**. **43c** was synthesized similar to **1c** and then reacted with **2a**, **11a**, or **14a** to produce **S06-1043** to **S06-1046**.

4.1.5.1. 2-(2-(4-Amino-1,2,5-oxadiazol-3-yl)-5,6-dimethyl-1H-benzo[d]imidazol-1-yl)-N-(quinolin-6-yl)acetamide (S06-1043). According to the general procedure described above, compound **S06-1043** was synthesized with **2a** and **43c**, with a yield of 48%, mp 279.5−282 °C, 96.7% HPLC purity. ^{1}H NMR (300 MHz, DMSO-d_6): δ = 10.90 (s, 1H), 8.78 (d, J = 2.61 Hz, 1H), 8.31 (s, 1H), 8.22 (d, J = 7.92 Hz, 1H), 8.00 (d, J = 9.39 Hz, 1H), 7.82 (dd, J = 3.96, 9.08 Hz, 1H), 7.62 (d, J = 4.41 Hz, 2H), 7.46 (dd, J = 4.14, 8.28 Hz, 1H), 7.01 (s, 2H), 5.60 (s, 2H), 2.37 (s, 3H), 2.37 (s, 3H) ppm. ^{13}C NMR (125 MHz, DMSO-d_6): δ = 166.1, 156.4, 149.6, 145.2, 140.9, 140.7, 138.8, 137.0, 135.9, 135.2, 134.5, 132.5, 130.2, 128.8, 123.5, 122.3, 120.1, 115.6, 111.4, 48.6, 20.7, 20.4 ppm. MS (ESI): calcd for $C_{22}H_{19}N_7O_2$ [M + H]$^+$ 414.1673; found, 414.1685.

4.1.5.2. 2-(2-(4-Amino-1,2,5-oxadiazol-3-yl)-5,6-dimethyl-1H-benzo[d]imidazol-1-yl)-N-(quinolin-3-yl)acetamide (S06-1044). Ac-

cording to the general procedure described above, compound **S06-1044** was synthesized with **11a** and **43c**, with a yield of 42%, mp 271−274 °C, 97.9% HPLC purity. ^{1}H NMR (300 MHz, DMSO-d_6): δ = 11.06 (s, 1H), 8.96 (d, J = 2.52 Hz, 1H), 8.63 (d, J = 2.31 Hz, 1H), 7.97 (d, J = 8.28 Hz, 1H), 7.87 (d, J = 7.32 Hz, 1H), 7.68−7.62 (m, 3H), 7.58−7.53 (m, 1H), 7.00 (s, 2H), 5.63 (s, 2H), 2.38 (s, 3H), 2.38 (s, 3H) ppm. ^{13}C NMR (125 MHz, DMSO-d_6): δ = 166.6, 156.4, 155.9, 144.8, 140.8, 140.6, 139.6, 138.8, 135.1, 134.5, 132.8, 132.5, 129.0, 128.2, 127.6, 122.7, 120.1, 111.3, 48.6, 20.7, 20.3 ppm. HRMS (m/z): calcd for $C_{22}H_{19}N_7O_2$ [M + H]$^+$ 414.1673; found, 414.1684.

4.1.5.3. 2-(2-(4-Amino-1,2,5-oxadiazol-3-yl)-5,6-dimethyl-1H-benzo[d]imidazol-1-yl)-N-(naphthalen-1-yl)acetamide (S06-1045). According to the general procedure described above, compound **S06-1045** was synthesized with **14a** and **43c**, with a yield of 38%, mp 279−282.5 °C, 98.4% HPLC purity. ^{1}H NMR (300 MHz, DMSO-d_6): δ = 10.51 (s, 1H), 8.24 (s, 1H), 7.96 (s, 1H), 7.78 (s, 1H), 7.61 (s, 5H), 7.48 (s, 1H), 7.00 (s, 2H), 5.70 (s, 2H), 2.39 (s, 3H), 2.36 (s, 3H) ppm. ^{13}C NMR (125 MHz, DMSO-d_6): δ = 166.6, 156.4, 140.9, 140.7, 138.8, 135.2, 134.5, 134.2, 133.5, 132.4, 128.6, 128.3, 126.6, 126.4, 126.1, 126.0, 123.2, 122.2, 120.1, 111.3, 48.5, 20.8, 20.3 ppm. HRMS (m/z): calcd for $C_{23}H_{20}N_6O_2$ [M + H]$^+$ 413.1721; found, 413.1739.

4.2. Biological Evaluation. *4.2.1. In Vitro AChE/BChE Inhibitory Evaluation.* The inhibitory activities of test compounds against AChE (EC 3.1.1.7) and BChE (EC 3.1.1.8) were carried out following the method of Ellman et al., using a Shimadzu 160 spectrophotometer. AChE (EC 3.1.1.7, Type VI-S, from electric eel, C3389), BChE (EC 3.1.1.8, from equine serum, C0663; from human, B4186), 5,5′-dithiobis (2-nitrobenzoic acid) (DTNB, D218200), acetylthiocholine iodide (ATC, A5751), and butyrylthiocholine iodide (BTC, B3253) were purchased from Sigma-Aldrich (St. Louis, MO). AChE/BChE stock solution was prepared by adjusting 500 units of the enzyme in gelatin solution (1% in deionized water) and further diluted with water to give the final concentrations of 2.5 units/mL (for eeAChE and eqBChE) or 0.015 units/mL (for hBChE). ATC/BTC iodide solutions were prepared with deionized water before using to give the concentration of 0.075 M. DTNB solution (0.01 M) was prepared in water containing 0.15% (w/v) sodium bicarbonate. The buffer solution was prepared with potassium dihydrogen phosphate (1.36 g, 10 mmol) in 100 mL of water. The pH of the solution was adjusted to 8.0 ± 0.1 with KOH. The test compounds were dissolved in DMSO to give a final concentration of 10^{-1} M to produce stock solutions. Subsequently, at least six different concentrations of each compound (normally 10^{-4}−10^{-9}, diluted with ethanol) were used to determine the ChE inhibitory activities.

The measurement was performed using a 96-well plate. Then, 40 μL of buffer, 10 μL of test compounds with different concentrations, 10 μL of AChE or BChE, and 20 μL of DTNB were added and mixed in a well. The solution in a 96-well plate was preincubated at room temperature for 5 min (for eeAChE and eqBChE) or 20 min (for hBChE). After the addition of 20 μL of ATC or BTC, the reaction was initiated. After 2 min of incubation at room temperature, the absorption was determined at 25 °C at 412 nm. The sample replacing the compound solution with 10 μL of ethanol was used to determine 100% of the enzyme activity. For determining the blank value, 10 μL of water replaced the enzyme solution. All of the measurements for each concentration were performed in triplicate and at least in three independent runs. The inhibition curve was fitted by plotting the percentage enzyme activity (100% for the reference) vs the logarithm of the test compound concentration. The IC$_{50}$ values were calculated by GraphPad Prism 6.0 software, and the data were expressed as the mean ± SD.

4.2.2. Molecular Modeling and Molecular Dynamics Studies. The docking study was performed by the CDOCKER module implemented in Discovery Studio 2019 (BIOVIA). CDOCKER is a grid-based molecular docking method that employs CHARMm. Briefly, random ligand conformations were generated by high-temperature molecular dynamics using a modified CHARMm forcefield (Prepare Ligands). The acquired structures were subsequently minimized under the same forcefield (Minimize Ligands). The solutions were then clustered based on the positions and conformations and ranked by energy. The cocrystal structure of hBChE bound with the reported screening-template compound was selected for molecular docking. The structure

was downloaded from Protein Data Bank (PDB id: 5k5e). The receptor was prepared by the "Prepare Protein" module in DS for further docking. A sphere (in 10 Å radius) around the original ligand was defined as the binding site. All other parameters were kept as default. After the docking procedure, 10 top-ranked conformations were obtained.

Molecular dynamics (MD) simulations were conducted after molecular docking to explore the dynamic binding process using the PMEMD module in AMBER 16. To start with, the previously obtained docking modes were imported and prepared with the AMBER ff99SB forcefield (for proteins), the ANTECHAMBER module, and the general AMBER forcefield (for ligands). Thereafter, hydrogen atoms of both the receptor and ligand were added using the "Reduce" module to ensure the integrity of simulations. The simulation systems were solvated in a TIP3P water box in a 9 Å hexahedron, and sodium ions were added to neutralize the systems. To reduce possible steric stresses, the minimum steps of the systems were set as 1000 in the way of the steepest descent method. Additionally, the conjugate gradient method was applied in another 1000 steps. The systems were then heated from 0 to 300 K in a linear way using a Langevin thermostat; the protein backbone atoms were exerted with a weak restraint of 10 kcal/mol over 1 ns. Finally, MD simulation of 100 ns in the NPT ensemble was set at 1 atm and 300 K. The MMGBSA method in AMBER 16 software was performed to calculate the binding free energies and energy decomposition.

4.2.3. Cell Culture and Treatments. All cells were purchased from the Cell Culture Center at the Institute of Basic Medical Sciences, Chinese Academy of Medical Sciences. Dulbecco's modified Eagle's medium (DMEM) and 3-(4,5-dimethylthiazol-2-yl)-2,5-diphenyltetrazolium (MTT) were purchased from Sigma (M2128, St. Louis, MO). Recombinant human 1,1,1,3,3,3-hexafluoro-2-propanol-pretreated $A\beta_{1-42}$ peptide was obtained from Merck Millipore (Darmastadt, Germany). H_2O_2 and β-glutamate were purchased from Aladdin.

Cells were cultured in DMEM supplemented with 10% fetal bovine serum, 100 U/mL penicillin, and 100 μg/mL streptomycin in a humidified incubator at 37 °C with 5% CO_2. The test compounds were prepared as stock solutions of 10^{-1} M in DMSO and were subsequently diluted to the test concentrations with DMEM. MTT was dissolved in phosphate-buffered saline (PBS) to a stock concentration of 5 mg/mL and stored at −20 °C. For the cytotoxic stimuli, the $A\beta_{1-42}$ peptide was dissolved in DMSO as a 5 mM stock solution and incubated for 24 h at 37 °C in PBS at a final concentration of 2 mg/mL to induce $A\beta_{1-42}$ aggregation.

4.2.4. Cell Viability Assay. Cells were seeded in 96-well plates (1 × 10^4 per well) and incubated overnight. After attachment, the cells were treated with DMEM or compounds at various concentrations for 24 h at 37 °C. Then, 15 μL of MTT solution was added into each well and incubated for 4 h. Then, the solution was removed and 100 μL of DMSO was added to dissolve the MTT formazan crystals. Thereafter, the absorbance values (OD values) of cell samples were read at 492 nm by a spectrophotometer. The percentage of cell viability was calculated using the following formula: cell viability (%) = $OD_{(compound-treated)}$/ $OD_{(DMEM-treated)}$ × 100%. All data were calculated from three independent experiments. The IC_{50} values were calculated by Graphpad Prism 6.0, and the data were expressed as mean ± SD.

4.2.5. Neuroprotective Effect. Generally, 80% confluent SH-SY5Y cells were seeded with 5000 cells per well into sterile 96-well plates and incubated for 24 h. The previous medium was removed; the cells were exposed to DMEM or the test compounds at different concentrations and preincubated for 2 h. Subsequently, H_2O_2 (200 μM, diluted with DMEM), glutamate (20 mM, dissolved in DMEM), or $A\beta_{1-42}$ (15 μM, diluted with DMEM) was added sequentially to induce cell insults. After 24 h, 15 μL of MTT was added to each well; the 96-well plates were incubated for another 4 h at 37 °C. The blue-purple crystal MTT formazan was dissolved in DMSO after discarding the supernatant. The absorbance was determined at 492 nm using a microplate reader. Percentages of cell protection against H_2O_2, glutamate, and $A\beta_{1-42}$ were calculated by considering the absorbance of the control cells (100% cell viability).

4.2.6. ROS Measurement. The intracellular ROS levels were determined with an oxidation-sensitive fluorescent probe, dichloro-dihydro-fluorescein diacetate (DCFH-DA). It passively diffuses into cells and is subsequently deacetylated by esterases to produce nonfluorescent DCFH. In the presence of ROS, DCFH reacts with ROS to form a fluorescent product dichlorofluorescein (DCF), which is trapped inside the cells. For this measurement, BV2 cells were seeded in 96-well plates at a density of 1 × 10^4 per well and incubated for 24 h at 37 °C. The cells were exposed to the test compounds at diverse concentrations and preincubated for 1 h and then treated with LPS (2.5 μg/mL) for an additional 24 h. Afterward, the harvested cells were washed with PBS (pH 7.2 ± 0.1) and incubated with DCFH-DA (diluted to give a final concentration of 5 μM with DMEM) for 30 min. Then, the DCFH-DA medium was removed; the cells were washed three times with DMEM before being observed under an inverted microscope. Tacrine and test compounds were correspondingly orally administered to mice in groups iii−ix.

4.2.7. In Vitro Blood−Brain Barrier (BBB) Permeation Assay. The ability of compounds to permeate into the brain was evaluated using a parallel artificial membrane permeation assay (PAMPA) for BBB according to the method described by Di et al. Commercial drugs, DMSO, and dodecane were obtained from Aladdin and Energy Chemical. Porcine brain lipid (PBL) was purchased from Avanti Polar Lipids. The donor microplate (96-well filter plate, poly(vinylidene difluoride) (PVDF) membrane, pore size 0.45 μM) and the acceptor microplate (indented 96-well plate) were both obtained from Millipore. The 96-well UV plate (COSTAR) was purchased from Corning Inc. The test compounds were initially dissolved in DMSO at a concentration of 5 mg/mL. Then, it was diluted 200-fold with a solution of PBS (pH 7.4 ± 0.1)/EtOH (70:30, V/V) to give a final concentration of 100 μg/mL. The filter membrane in the donor microplate was impregnated with 4 μL of PBL in dodecane (20 mg/ mL). Thereafter, 200 μL of the diluted compound solution and 300 μL of PBS/EtOH (70:30, V/V) were added into the donor wells and the acceptor wells, respectively. The donor filter plate was carefully placed on the acceptor plate to form a "sandwich," making the filter membrane contact the buffer solution. The sandwich assembly was left undisturbed for 18 h at 25 °C. After that, the donor plate was carefully removed; the concentrations of test compounds in the donor and acceptor wells were measured with a UV plate spectroscopy reader (SpectraMax Plus 384, Molecular Devices, Sunnyvale, CA). Each sample was analyzed at five wavelengths, in at least three independent runs, in four wells, and the results are given as the means ± SD. In each experiment, nine quality control standards of known BBB permeability were included to validate the analysis set.

4.2.8. Liver Microsome Stability Assay and Metabolites Analysis. All liver microsome assays were performed by Shanghai ChemPartner Co., Ltd. Metabolic stability of testing compounds was evaluated using human liver microsomes to predict intrinsic clearance. The assay was conducted in 96-well plates at 37 °C. The solution (45 μL) contained a final concentration of 1 μM test compound, 0.5 mg/mL liver microsome protein, and 2 mM NADPH. At each of the time points (0-, 5-, 15-, 30-, and 45-min), 135 μL of acetonitrile containing an internal standard (imipramine) was transferred to corresponding wells to stop the reaction. Ketanserin was included as the positive control to validate the assay performance.[57] Plates were sealed, shaken (600 rpm for 10 min), and then centrifuged at 4 °C at 5500*g* for 15 min. Then, 50 μL of the supernatant was transferred into a fresh 96-well sample plate containing 50 μL of ultrapure water (Millipore, ZMQS50F01) for liquid chromatography with tandem mass spectrometry (LC/MS/MS) analysis. All samples were analyzed on LC/MS/MS using an API 4000 instrument. Analytical samples were separated using an Ultimate-XB-C18 (5 μm, 2.1 × 50 mm²) at a flow rate of 0.6 mL/min. The mobile phase consists of 0.025% formic acid in water (as solvent A) and methanol (as solvent B). The metabolism extent was calculated as the clearance of compounds, compared to the 0 min time incubation. Initial rates were calculated for the compound concentration and used to determine $t_{1/2}$ values and the intrinsic clearance.

Metabolite analysis was evaluated using human liver microsomes. The assay was conducted in 96-well plates at 37 °C. The solution

contained a final concentration of 20 μM test compound, 1 mg/mL liver microsome protein, 10 mM $MgCl_2$, 1 mM NADPH, 10 mM G-6-P, and 1.0 unit/mL PDH. After 120 min, a triple amount of acetonitrile was added to stop the reaction. The plate was sealed, shaken, and then centrifuged at 4 °C at 5500g for 15 min. Then, 50 μL of the supernatant was transferred into a fresh 96-well sample plate containing 50 μL of ultrapure water (Millipore, ZMQS50F01) for LC/MS/MS analysis. The analysis approach was the same as that of the stability assay.

4.2.9. In Vivo PK Study. The study was conducted in the Pharmaceutical Laboratory Animal Center of China Pharmaceutical University (IACUC). The experiment meets the ethical considerations. Healthy male Sprague−Dawley rats (180−220 g, Nanjing Qinglong-shan Animal Breeding Factory, China) were randomly divided into two groups ($n = 8$) to analyze PK properties of the test compound. Eight rats were used for oral administration (10 mg/kg), while the other eight rats were used for intravenous administration (10 mg/kg). The compound sample was dissolved in a mixture of DMSO, poly(ethylene glycol) (PEG) 400, and normal saline (10:80:10, V/V/V) before the experiments. The animals were fasted overnight before initiating the experiment but had free access to water. After administration, the blood samples were collected from the retro-orbital plexus at 1, 5, 10, 20, 30, 60, 120, 240, 360, 480, 720, and 1440 min into heparinized tubes. Blood samples were immediately centrifuged at 8000 rpm for 10 min to separate the plasma. Then, 100 μL of plasma was precipitated by addition of 300 μL of chromatographic methanol containing an internal standard (theophylline), vortexed for 10 min, and centrifuged at 15 000 rpm for 10 min. The supernatant (100 μL) was collected and transferred into HPLC vials for LC/MS/MS to determine the concentrations in plasma, using the mobile phase consisting of an aqueous solution containing 0.1% formic acid (as solvent A, 30%) and methanol (as solvent B, 70%) at a flow rate of 0.6 mL/min using a Hedera ODS-2 column (5 μm, 2.1 × 50 mm^2). The standard curve was generated by the addition of serial concentrations of compound with an internal standard to blank plasma. The PK parameters were calculated using the plasma concentration data of the test compound at different time points using extravascular analysis of the noncompartmental (NCA) model with PK Solver software.

4.2.10. In Vivo BBB Penetration Determination. The study was conducted in the Pharmaceutical Laboratory Animal Center of China Pharmaceutical University (IACUC). The experiment meets the ethical considerations. Compound **S06-1011** was dissolved in 5% DMSO, 40% PEG 400, and 55% saline to yield a nominal concentration of 1 mg/mL and was dosed at 10 mg/kg in ICR mice by oral administration. Samples were collected at 30, 60, 120, and 240 min postdose. Mice were anesthetized and sacrificed, blood was collected by retro-orbital bleeds, and brains were collected. Blood samples were processed and analyzed as described above. Brain samples were mixed with a double volume of PBS and fully homogenized. Subsequently, a triple volume of ethyl acetate was added and vortexed for 2 min. The mixture was centrifuged at 15 000 rpm for 10 min, and the supernatant (1000 μL) was collected. The solvent was allowed to evaporate in the fume hood, and the residue was reconstituted with the mobile phase (250 μL). The samples were analyzed as described above.

4.2.11. Acute Toxicity Evaluation. The study was conducted in the Pharmaceutical Laboratory Animal Center of China Pharmaceutical University (IACUC). The experiment meets the ethical considerations. Three test compounds were serially suspended in 5% DMSO, 40% PEG 400, and 55% saline. Forty male and forty female mice (15−18 g) were divided into eight groups ($n = 9$): male control group, female control group, and male test groups for three compounds, and female test groups for three compounds. All mice had been fasted overnight, and then the mice in test groups were intragastrically administered with a dosage of 1 g/kg of test compounds while the mice in control groups were administered with the same volume of vehicle solution on the first day. The death, daily behavior, and body mass were monitored during the subsequent 2 weeks. All mice were dissected on day 14, and the liver was extracted and then examined by HE to see if any damages occurred.

4.2.12. Behavioral Study I (Scopolamine as the Modeling Stimuli). The study was conducted in the Pharmaceutical Laboratory Animal Center of China Pharmaceutical University (IACUC). The experiment

meets the ethical considerations. The experiment was performed using ICR male mice (8−10 weeks old, weight 18−20 g), which were purchased from Nanjing Qinglongshan Animal Breeding Factory (Nanjing, China). The modeling stimulus, scopolamine, was obtained from Aladdin. Tacrine, used as the positive control, was purchased from Sigma. The cognitive function of mice was evaluated by the Morris water maze analysis-management system (Viewer2 Tracking Software, Ji Liang Instruments, Shanghai, China) to record the escape latency and the trajectory to the platform.[58] The test compounds were suspended in a mixture of DMSO and normal saline (10:90, V/V) before the experiments.

The mice were separated into nine groups as follows ($n = 8$): (i) vehicle as the blank control group, (ii) scopolamine (3 mg/kg, intraperitoneal injection) as the model group, (iii) tacrine (15 mg/kg, intragastric administration) + scopolamine (3 mg/kg, intraperitoneal injection) as the positive control group, (iv) test compound **S06-1011** (15 mg/kg, intragastric administration) + scopolamine (3 mg/kg, intraperitoneal injection) group, (v) test compound **S06-1011** (30 mg/kg, intragastric administration) + scopolamine (3 mg/kg, intraperitoneal injection) group, (vi) test compound **S06-1015** (15 mg/kg, intragastric administration) + scopolamine (3 mg/kg, intraperitoneal injection) group, (vii) test compound **S06-1015** (30 mg/kg, intragastric administration) + scopolamine (3 mg/kg, intraperitoneal injection) group, (viii) test compound **S06-1031** (15 mg/kg, intragastric administration) + scopolamine (3 mg/kg, intraperitoneal injection) group, and (ix) test compound **S06-1031** (30 mg/kg, intragastric administration) + scopolamine (3 mg/kg, intraperitoneal injection) group. Tacrine and test compounds were correspondingly orally administered to mice in groups iii−ix, 30 min before the intraperitoneal injection of scopolamine for 10 consecutive days.

During the last 5 days, spatial learning and memory were evaluated by the Morris water maze. The maze was placed in a lit room with visual cues at 25 °C. A platform (6 cm radius, 1.0 cm submerged under the water level) was put in the center of one quadrant of the circular pool (60 cm radius, 45 cm height) with a depth of 30 cm water. The behavioral study of each mouse consisted of 5 days of learning and memory training and a probe trail on day 6. The mice started facing the pool wall and were pseudorandomized for each trial. For cognitive evaluation, each mouse was separately evaluated by a visible platform (days 1−2) and a hidden platform (days 3−5) of the water maze. Mice received a nonspatial pretraining during the training days 1−2, prepared for the subsequent spatial learning test. During these 2 days, mice were trained to find the platform that was labeled by a small flag. On days 3−5, the hidden-platform version was used to explore the retention of memory to find the platform. The hidden platform was placed 1 cm below the water level. All mice were subjected to two trials, each of which was lasting 90 s. The mouse successfully reaching the platform was called "a successful escape", and its escape latency was recorded. If a mouse failed to arrive at the platform within 90 s, the test was terminated. The mouse was navigated to the platform by hand and got used to the platform for 1 min. On the last day (day 6), the platform was removed from its location and the probe trial was performed. The escape latency and the traveled trajectory of all mice were recorded by Panlab SMART 3.0 and processed by Graphpad Prism 6.0 software.

4.2.13. Behavioral Study II (Oligomerized Aβ_{1-42} as the Modeling Stimuli). The study was conducted in the Pharmaceutical Laboratory Animal Center of China Pharmaceutical University (IACUC). The experiment meets the ethical considerations. ICR mice (6−8 weeks old, 18−22 g, Nanjing Qinglongshan Animal Breeding Factory, China) were separated into seven groups ($n = 8$) for this experiment. Recombinant human 1,1,1,3,3,3-hexafluoro-2-propanol-pretreated Aβ_{1-42} peptide was obtained from Merck Millipore (Darmastadt, Germany). Aβ_{1-42} peptide was dissolved in DMSO as a 5 mM stock solution and incubated for 24 h at 37 °C in normal saline at a final concentration of 2 mg/mL to induce Aβ_{1-42} aggregation.[59] Donepezil, used as the positive control, was purchased from Sigma. The cognitive function was evaluated by the Morris water maze and the Y maze, using a computer equipped with an analysis-management system (Viewer2 Tracking Software, Ji Liang Instruments, Shanghai, China). The test

compounds were suspended in a mixture of DMSO and normal saline (10:90, V/V) before the experiments.

The oligomerized $A\beta_{1-42}$ peptide was injected (intracerebroventricular injection, icv) on the first day of the experiment, and test compounds were intragastrically injected during days 2−14. The mice were grouped as follows (n = 8): (i) vehicle (intragastric administration) as the blank control group; (ii) oligomerized $A\beta_{1-42}$ peptide (10 μg per mouse, icv) as the model group; (iii) normal saline (icv) as the sham-operation group; (iv) oligomerized $A\beta_{1-42}$ peptide (10 μg per mouse, icv) + donepezil (15 mg/kg, intragastric administration) as the positive control group; (v) oligomerized $A\beta_{1-42}$ peptide (10 μg per mouse, icv) + test compound **S06-1011** (15 mg/kg, intragastric administration) group; (vi) oligomerized $A\beta_{1-42}$ peptide (10 μg per mouse, icv) + test compound **S06-1015** (15 mg/kg, intragastric administration) group; and (vii) oligomerized $A\beta_{1-42}$ peptide (10 μg per mouse, icv) + test compound **S06-1031** (15 mg/kg, intragastric administration) group. The behavioral studies included the Morris water maze on days 9−14 and the Y maze on day 15.

The Morris water maze was performed like described before (in section Section 4.2.12). The spatial learning and memory were conducted on days 9−13, and the probe trail was performed on day 14.

On day 15, all mice were tested for spontaneous alternation performance in the Y maze to define the spatial working memory.[27,60] The Y maze assembly was made of gray poly(vinyl chloride), with three arms (40 cm long, 13 cm high, 3 cm wide at the bottom, 10 cm wide at the top, converging at an angle of 120°). Each mouse was placed at the end of one arm and explored freely in the maze for 5 min. The sequence of arm entries of the Y maze was checked visually and recorded. The mouse entering the three arms on consecutive occasions was defined as an alternation. The total number of arm entries minus two was the maximum alternation. The percentage of alternation performance was calculated as (actual alternations/maximum alternations) × 100%. If an extreme behavior (alternation percentage <20 or >90%) occurs, this alternation was not involved. All values were expressed as means ± SD by Graphpad Prism 6.0 software.

■ ASSOCIATED CONTENT

Ⓢ Supporting Information

The Supporting Information is available free of charge at https://pubs.org/doi/10.1021/acs.jmedchem.1c00167.

- Molecular dynamics—8012-9656 (PDB)
- Molecular dynamics—**S06-1002** (PDB)
- Molecular dynamics—**S06-1011** (PDB)
- Molecular dynamics—**S06-1014** (PDB)
- Molecular string formulas (CSV)
- Compound characterization; inhibitory rates on *ee*AChE and on *eq*BChE of partial compounds; molecular docking modes of **S06-1002**, **S06-1011**, and **S06-1014**; molecular dynamic simulation results of **S06-1001**, **S06-1002**, **S06-1011**, and **S06-1014**; chromatographic and mass spectrometric identification information for **S06-1011**; standard curves for pharmacokinetics and PAMPA study; quantization of ROS production; protocol for the *in vivo* experiments (PDF)

■ AUTHOR INFORMATION

Corresponding Authors

Wenyuan Liu − *School of Pharmacy, China Pharmaceutical University, Nanjing 211198, People's Republic of China*; Phone: +86-18012955795; Email: liuwenyuan@cpu.edu.cn

Yao Chen − *School of Pharmacy, Nanjing University of Chinese Medicine, Nanjing 210023, People's Republic of China*; Phone: +86-13921442470; Email: clarissa0710@163.com, 300630@njucm.edu.cn

Haopeng Sun − *School of Pharmacy, China Pharmaceutical University, Nanjing 211198, People's Republic of China*; ⓘ orcid.org/0000-0002-5109-0304; Phone: +86-13951934235; Email: sunhaopeng@163.com

Authors

Qi Li − *School of Pharmacy, China Pharmaceutical University, Nanjing 211198, People's Republic of China; School of Basic Medicine, Qingdao University, Qingdao 266071, People's Republic of China*

Ying Chen − *Department of Natural Medicinal Chemistry, China Pharmaceutical University, Nanjing 211198, People's Republic of China*

Shuaishuai Xing − *School of Pharmacy, China Pharmaceutical University, Nanjing 211198, People's Republic of China*

Qinghong Liao − *Department of Natural Medicinal Chemistry, China Pharmaceutical University, Nanjing 211198, People's Republic of China*

Baichen Xiong − *School of Pharmacy, China Pharmaceutical University, Nanjing 211198, People's Republic of China*

Yuanyuan Wang − *School of Pharmacy, China Pharmaceutical University, Nanjing 211198, People's Republic of China*

Weixuan Lu − *School of Pharmacy, China Pharmaceutical University, Nanjing 211198, People's Republic of China*

Siyu He − *State Key Laboratory of Natural Medicines, Jiangsu Key Laboratory of Carcinogenesis and Intervention, School of Basic Medicine and Clinical Pharmacy, China Pharmaceutical University, Nanjing 210009, People's Republic of China*

Feng Feng − *Department of Natural Medicinal Chemistry, China Pharmaceutical University, Nanjing 211198, People's Republic of China; Jiangsu Food and Pharmaceutical Science College, Huai'an 223003, People's Republic of China*

Complete contact information is available at:
https://pubs.acs.org/10.1021/acs.jmedchem.1c00167

Notes

The authors declare no competing financial interest.

■ ACKNOWLEDGMENTS

■ ABBREVIATIONS

AD, Alzheimer's disease; β-amyloid, $A\beta$; NMDAR, *N*-methyl-D-aspartic acid receptor; ChE, cholinesterases; ACh, acetylcholine; AChE, acetylcholinesterase; BChE, butyrylcholinesterase; CNS, central nervous system; BBB, blood−brain barrier; *ee*AChE, *electrophorus electricus* AChE; *eq*BChE, *equine serum* BChE; CAS, catalytic active site; PAS, peripheral anionic site; *h*AChE, human AChE; *h*BChE, human BChE; MD, molecular dynamics; IR, inhibitory rates; LE, ligand efficiency; MTT, 3-(4,5-dimethylthiazol-2-yl)-2,5-diphenyltetrazolium; AST, aspartate aminotransferase; ALT, alanine aminotransferase; HE, hematoxylin−eosin; PK, pharmacokinetics; PAMPA−BBB, parallel artificial membrane permeation assay of the blood−brain barrier; BBB, blood−brain barrier; C_{max}, peak exposure; AUC, area under the concentration−time curve; ROS, reactive oxygen

species; LPS, lipopolysaccharides; GFI, green fluorescence intensity; TLC, thin-layer chromatography; HPLC, high-performance liquid chromatography; DMEM, Dulbecco's modified Eagle's medium; PBS, phosphate-buffered saline; PEG, poly(ethylene glycol)

■ REFERENCES

(1) Blennow, K.; de Leon, M. J.; Zetterberg, H. Alzheimer's disease. *Lancet* **2006**, *368*, 387−403.

(2) Iqbal, K.; Grundke-Iqbal, I. Alzheimer disease is multifactorial and heterogeneous. *Neurobiol. Aging* **2000**, *21*, 901−904.

(3) Holzgrabe, U.; Kapkova, P.; Alptuzun, V.; Scheiber, J.; Kugelmann, E. Targeting acetylcholinesterase to treat neurodegeneration. *Expert Opin. Ther. Targets* **2007**, *11*, 161−179.

(4) Terry, R. D.; Gonatas, N. K.; Weiss, M. Ultrastructural Studies in Alzheimer's Presenile Dementia. *Am. J. Pathol.* **1964**, *44*, 269−297.

(5) Grundke-Iqbal, I.; Iqbal, K.; Tung, Y. C.; Quinlan, M.; Wisniewski, H. M.; Binder, L. I. Abnormal phosphorylation of the microtubule-associated protein tau (tau) in Alzheimer cytoskeletal pathology. *Proc. Natl. Acad. Sci. U.S.A.* **1986**, *83*, 4913−4917.

(6) Linker, R. A.; Lee, D. H.; Ryan, S.; van Dam, A. M.; Conrad, R.; Bista, P.; Zeng, W.; Hronowsky, X.; Buko, A.; Chollate, S.; Ellrichmann, G.; Bruck, W.; Dawson, K.; Goelz, S.; Wiese, S.; Scannevin, R. H.; Lukashev, M.; Gold, R. Fumaric acid esters exert neuroprotective effects in neuroinflammation via activation of the Nrf2 antioxidant pathway. *Brain* **2011**, *134*, 678−692.

(7) Aliev, G.; Priyadarshini, M.; Reddy, V. P.; Grieg, N. H.; Kaminsky, Y.; Cacabelos, R.; Ashraf, G. M.; Jabir, N. R.; Kamal, M. A.; Nikolenko, V. N.; Zamyatnin, A. A., Jr; Benberin, V. V.; Bachurin, S. O. Oxidative stress mediated mitochondrial and vascular lesions as markers in the pathogenesis of Alzheimer disease. *Curr. Med. Chem.* **2014**, *21*, 2208−2217.

(8) Kryger, G.; Silman, I.; Sussman, J. L. Structure of acetylcholinesterase complexed with E2020 (Aricept): implications for the design of new anti-Alzheimer drugs. *Structure* **1999**, *7*, 297−307.

(9) Greenblatt, H. M.; Kryger, G.; Lewis, T.; Silman, I.; Sussman, J. L. Structure of acetylcholinesterase complexed with (-)-galanthamine at 2.3 A resolution. *FEBS Lett.* **1999**, *463*, 321−326.

(10) Farlow, M. R.; Small, G. W.; Quarg, P.; Krause, A. Efficacy of rivastigmine in Alzheimer's disease patients with rapid disease progression: results of a meta-analysis. *Dementia Geriatr. Cognit. Disord.* **2005**, *20*, 192−197.

(11) Molino, I.; Colucci, L.; Fasanaro, A. M.; Traini, E.; Amenta, F. Efficacy of Memantine, Donepezil, or Their Association in Moderate-Severe Alzheimer's Disease: A Review of Clinical Trials. *Sci. World J.* **2013**, *2013*, No. 925702.

(12) Deutsch, J. A. The cholinergic synapse and the site of memory. *Science* **1971**, *174*, 788−794.

(13) Fibiger, H. C. Cholinergic mechanisms in learning, memory and dementia: a review of recent evidence. *Trends Neurosci.* **1991**, *14*, 220−223.

(14) Schliebs, R. Basal forebrain cholinergic dysfunction in Alzheimer's disease - Interrelationship with beta-amyloid, inflammation and neurotrophin signaling. *Neurochem. Res.* **2005**, *30*, 895−908.

(15) Bartus, R. T. On neurodegenerative diseases, models, and treatment strategies: Lessons learned and lessons forgotten a generation following the cholinergic hypothesis. *Exp. Neurol.* **2000**, *163*, 495−529.

(16) Chatonnet, A.; Lockridge, O. Comparison of butyrylcholinesterase and acetylcholinesterase. *Biochem. J.* **1989**, *260*, 625−634.

(17) Ariel, N.; Ordentlich, A.; Barak, D.; Bino, T.; Velan, B.; Shafferman, A. The 'aromatic patch' of three proximal residues in the human acetylcholinesterase active centre allows for versatile interaction modes with inhibitors. *Biochem. J.* **1998**, *335*, 95−102.

(18) Mesulam, M. M.; Guillozet, A.; Shaw, P.; Levey, A.; Duysen, E. G.; Lockridge, O. Acetylcholinesterase knockouts establish central cholinergic pathways and can use butyrylcholinesterase to hydrolyze acetylcholine. *Neuroscience* **2002**, *110*, 627−639.

(19) Xie, W.; Stribley, J. A.; Chatonnet, A.; Wilder, P. J.; Rizzino, A.; McComb, R. D.; Taylor, P.; Hinrichs, S. H.; Lockridge, O. Postnatal developmental delay and supersensitivity to organophosphate in gene-targeted mice lacking acetylcholinesterase. *J. Pharmacol. Exp. Ther.* **2000**, *293*, 896−902.

(20) Perry, E. K.; Perry, R. H.; Blessed, G.; Tomlinson, B. E. Changes in brain cholinesterases in senile dementia of Alzheimer type. *Neuropathol. Appl. Neurobiol.* **1978**, *4*, 273−277.

(21) Li, Q.; He, S.; Chen, Y.; Feng, F.; Qu, W.; Sun, H. Donepezil-based multi-functional cholinesterase inhibitors for treatment of Alzheimer's disease. *Eur. J. Med. Chem.* **2018**, *158*, 463−477.

(22) Li, B.; Duysen, E. G.; Carlson, M.; Lockridge, O. The butyrylcholinesterase knockout mouse as a model for human butyrylcholinesterase deficiency. *J. Pharmacol. Exp. Ther.* **2008**, *324*, 1146−1154.

(23) Manoharan, I.; Boopathy, R.; Darvesh, S.; Lockridge, O. A medical health report on individuals with silent butyrylcholinesterase in the Vysya community of India. *Clin. Chim. Acta* **2007**, *378*, 128−135.

(24) Xing, S.; Li, Q.; Xiong, B.; Chen, Y.; Feng, F.; Liu, W.; Sun, H. Structure and therapeutic uses of butyrylcholinesterase: Application in detoxification, Alzheimer's disease, and fat metabolism. *Med. Res. Rev.* **2021**, *41*, 858−901.

(25) Gómez-Ramos, P.; Moran, M. A. Ultrastructural localization of butyrylcholinesterase in senile plaques in the brains of aged and Alzheimer disease patients. *Mol. Chem. Neuropathol.* **1997**, *30*, 161−173.

(26) Reid, G. A.; Darvesh, S. Butyrylcholinesterase-knockout reduces brain deposition of fibrillar beta-amyloid in an Alzheimer mouse model. *Neuroscience* **2015**, *298*, 424−435.

(27) Maurice, T.; Strehaiano, M.; Simeon, N.; Bertrand, C.; Chatonnet, A. Learning performances and vulnerability to amyloid toxicity in the butyrylcholinesterase knockout mouse. *Behav. Brain Res.* **2016**, *296*, 351−360.

(28) Kuroda, A.; Setoguchi, M.; Uchino, Y.; Nagata, K.; Hokonohara, D. Effect of rivastigmine on plasma butyrylcholine esterase activity and plasma ghrelin levels in patients with dementia in Alzheimer's disease. *Geriatr. Gerontol. Int.* **2018**, *18*, 886−891.

(29) Tsuno, N.; Mori, T.; Ishikawa, I.; Bando, N.; Park, H.; Matsumoto, Y.; Mori, I.; Tanaka, M.; Hirano, T.; Nakamura, Y. Efficacy of rivastigmine transdermal therapy on low food intake in patients with Alzheimer's disease: The Attitude Towards Food Consumption in Alzheimer's Disease Patients Revive with Rivastigmine Effects study. *Geriatr. Gerontol. Int.* **2019**, *19*, 571−576.

(30) Jimenez, A.; Pegueroles, J.; Carmona-Iragui, M.; Vilaplana, E.; Montal, V.; Alcolea, D.; Videla, L.; Illan-Gala, I.; Pane, A.; Casajoana, A.; Belbin, O.; Clarimon, J.; Moize, V.; Vidal, J.; Lleo, A.; Fortea, J.; Blesa, R.; Alzheimer's Disease Neuroimaging Initiative. Weight loss in the healthy elderly might be a non-cognitive sign of preclinical Alzheimer's disease. *Oncotarget* **2017**, *8*, 104706−104716.

(31) Gurevitz, S. L.; Costakis, T.; Leiter, J. Do atypical antipsychotics cause weight gain in nursing home dementia residents? *Consult. Pharm.* **2004**, *19*, 809−812.

(32) Brimijoin, S.; Chen, V. P.; Pang, Y. P.; Geng, L.; Gao, Y. Physiological roles for butyrylcholinesterase: A BChE-ghrelin axis. *Chem.-Biol. Interact.* **2016**, *259*, 271−275.

(33) Mear, Y.; Enjalbert, A.; Thirion, S. GHS-R1a constitutive activity and its physiological relevance. *Front. Neurosci.* **2013**, *7*, No. 87.

(34) Quiñones, M.; Ferno, J.; Al-Massadi, O. Ghrelin and liver disease. *Rev. Endocr. Metab. Disord.* **2020**, *21*, 45−56.

(35) Dickson, S. L.; Leng, G.; Robinson, I. C. Systemic administration of growth hormone-releasing peptide activates hypothalamic arcuate neurons. *Neuroscience* **1993**, *53*, 303−306.

(36) Castañeda, T. R.; Tong, J.; Datta, R.; Culler, M.; Tschop, M. H. Ghrelin in the regulation of body weight and metabolism. *Front Neuroendocrinol.* **2010**, *31*, 44−60.

(37) Korbonits, M.; Goldstone, A. P.; Gueorguiev, M.; Grossman, A. B. Ghrelin–a hormone with multiple functions. *Front. Neuroendocrinol.* **2004**, *25*, 27−68.

(38) Ferrini, F.; Salio, C.; Lossi, L.; Merighi, A. Ghrelin in central neurons. *Curr. Neuropharmacol.* **2009**, *7*, 37−49.

(39) Li, Q.; Xing, S.; Chen, Y.; Liao, Q.; Xiong, B.; He, S.; Lu, W.; Liu, Y.; Yang, H.; Li, Q.; Feng, F.; Liu, W.; Chen, Y.; Sun, H. Discovery and Biological Evaluation of a Novel Highly Potent Selective Butyrylcholinsterase Inhibitor. *J. Med. Chem.* **2020**, *63*, 10030−10044.

(40) Li, Q.; Yang, H.; Chen, Y.; Sun, H. Recent progress in the identification of selective butyrylcholinesterase inhibitors for Alzheimer's disease. *Eur. J. Med. Chem.* **2017**, *132*, 294−309.

(41) Davis, L.; Britten, J. J.; Morgan, M. Cholinesterase. Its significance in anaesthetic practice. *Anaesthesia* **1997**, *52*, 244−260.

(42) Park, J. W.; Ha, Y. M.; Moon, K. M.; Kim, S. R.; Jeong, H. O.; Park, Y. J.; Lee, H. J.; Park, J. Y.; Song, Y. M.; Chun, P.; Byun, Y.; Moon, H. R.; Chung, H. Y. De novo tyrosinase inhibitor: 4-(6,7-dihydro-5H-indeno[5,6-d]thiazol-2-yl)benzene-1,3-diol (MHY1556). *Bioorg. Med. Chem. Lett.* **2013**, *23*, 4172−4176.

(43) Di, L.; Kerns, E. H.; Fan, K.; McConnell, O. J.; Carter, G. T. High throughput artificial membrane permeability assay for blood-brain barrier. *Eur. J. Med. Chem.* **2003**, *38*, 223−232.

(44) Li, Q.; Xing, S.; Chen, Y.; Liao, Q.; Li, Q.; Liu, Y.; He, S.; Feng, F.; Chen, Y.; Zhang, J.; Liu, W.; Guo, Q.; Sun, Y.; Sun, H. Reasonably activating Nrf2: A long-term, effective and controllable strategy for neurodegenerative diseases. *Eur. J. Med. Chem.* **2020**, *185*, No. 111862.

(45) Zhang, L.; Zhao, B.; Yew, D. T.; Kusiak, J. W.; Roth, G. S. Processing of Alzheimer's amyloid precursor protein during H2O2-induced apoptosis in human neuronal cells. *Biochem. Biophys. Res. Commun.* **1997**, *235*, 845−848.

(46) Murphy, T. H.; Miyamoto, M.; Sastre, A.; Schnaar, R. L.; Coyle, J. T. Glutamate toxicity in a neuronal cell line involves inhibition of cystine transport leading to oxidative stress. *Neuron* **1989**, *2*, 1547−1558.

(47) Brus, B.; Kosak, U.; Turk, S.; Pislar, A.; Coquelle, N.; Kos, J.; Stojan, J.; Colletier, J. P.; Gobec, S. Discovery, biological evaluation, and crystal structure of a novel nanomolar selective butyrylcholinesterase inhibitor. *J. Med. Chem.* **2014**, *57*, 8167−8179.

(48) Kayed, R.; Head, E.; Thompson, J. L.; McIntire, T. M.; Milton, S. C.; Cotman, C. W.; Glabe, C. G. Common structure of soluble amyloid oligomers implies common mechanism of pathogenesis. *Science* **2003**, *300*, 486−489.

(49) Jin, M.; Shepardson, N.; Yang, T.; Chen, G.; Walsh, D.; Selkoe, D. J. Soluble amyloid beta-protein dimers isolated from Alzheimer cortex directly induce Tau hyperphosphorylation and neuritic degeneration. *Proc. Natl. Acad. Sci. U.S.A.* **2011**, *108*, 5819−5824.

(50) Shoffner, J. M. Oxidative phosphorylation defects and Alzheimer's disease. *Neurogenetics* **1997**, *1*, 13−19.

(51) Schubert, D.; Behl, C.; Lesley, R.; Brack, A.; Dargusch, R.; Sagara, Y.; Kimura, H. Amyloid peptides are toxic via a common oxidative mechanism. *Proc. Natl. Acad. Sci. U.S.A.* **1995**, *92*, 1989−1993.

(52) Sinha, S.; Lieberburg, I. Cellular mechanisms of beta-amyloid production and secretion. *Proc. Natl. Acad. Sci. U.S.A.* **1999**, *96*, 11049−11053.

(53) Wang, Y.; Qin, Z. H. Molecular and cellular mechanisms of excitotoxic neuronal death. *Apoptosis* **2010**, *15*, 1382−1402.

(54) Pawate, S.; Shen, Q.; Fan, F.; Bhat, N. R. Redox regulation of glial inflammatory response to lipopolysaccharide and interferongamma. *J. Neurosci. Res.* **2004**, *77*, 540−551.

(55) Dolev, I.; Michaelson, D. M. A nontransgenic mouse model shows inducible amyloid-beta (Abeta) peptide deposition and elucidates the role of apolipoprotein E in the amyloid cascade. *Proc. Natl. Acad. Sci. U.S.A.* **2004**, *101*, 13909−13914.

(56) Lahmy, V.; Meunier, J.; Malmstrom, S.; Naert, G.; Givalois, L.; Kim, S. H.; Villard, V.; Vamvakides, A.; Maurice, T. Blockade of Tau hyperphosphorylation and Abeta(1)(-)(4)(2) generation by the aminotetrahydrofuran derivative ANAVEX2-73, a mixed muscarinic and sigma(1) receptor agonist, in a nontransgenic mouse model of Alzheimer's disease. *Neuropsychopharmacology* **2013**, *38*, 1706−1723.

(57) Akabane, T.; Gerst, N.; Naritomi, Y.; Masters, J. N.; Tamura, K. A practical and direct comparison of intrinsic metabolic clearance of several non-CYP enzyme substrates in freshly isolated and cryopreserved hepatocytes. *Drug Metab. Pharmacokinet.* **2012**, *27*, 181−191.

(58) Zha, X.; Lamba, D.; Zhang, L.; Lou, Y.; Xu, C.; Kang, D.; Chen, L.; Xu, Y.; Zhang, L.; De Simone, A.; Samez, S.; Pesaresi, A.; Stojan, J.; Lopez, M. G.; Egea, J.; Andrisano, V.; Bartolini, M. Novel Tacrine-Benzofuran Hybrids as Potent Multitarget-Directed Ligands for the Treatment of Alzheimer's Disease: Design, Synthesis, Biological Evaluation, and X-ray Crystallography. *J. Med. Chem.* **2016**, *59*, 114−131.

(59) Maurice, T.; Lockhart, B. P.; Privat, A. Amnesia induced in mice by centrally administered beta-amyloid peptides involves cholinergic dysfunction. *Brain Res.* **1996**, *706*, 181−193.

(60) Dolles, D.; Hoffmann, M.; Gunesch, S.; Marinelli, O.; Moller, J.; Santoni, G.; Chatonnet, A.; Lohse, M. J.; Wittmann, H. J.; Strasser, A.; Nabissi, M.; Maurice, T.; Decker, M. Structure-Activity Relationships and Computational Investigations into the Development of Potent and Balanced Dual-Acting Butyrylcholinesterase Inhibitors and Human Cannabinoid Receptor 2 Ligands with Pro-Cognitive in Vivo Profiles. *J. Med. Chem.* **2018**, *61*, 1646−1663.